Leukocytes have a heparan sulfate glycocalyx that regulates recruitment during psoriasis-like skin inflammation

Megan J. Priestley,^{1,2} Anna K. Hains,¹ Iashia Z. Mulholland,¹ Sam Spijkers-Shaw,^{3,4} Joshua C. Müller^{5,6}, Gareth Howell⁷, Amanda J. L. Ridley¹, H. Davies-Strickleton¹, Rebecca L. Miller⁸, Max Nobis^{6,9}, Olga V. Zubkova⁴, Amy E. Saunders^{10*†} Douglas P. Dyer^{1,11*†}

¹Manchester Cell-Matrix Centre, Lydia Becker Institute of Immunology and Inflammation, Faculty of Biology, Medicine and Health, Manchester Academic Health Science Centre, University of Manchester; Manchester, M13 9PT, UK. ²Koch Institute for Integrative Cancer Research, Massachusetts Institute of Technology; Boston, MA, 02139, USA. ³Department of Chemistry and Chemical Biology, Northeastern University; Boston, MA, 02115, USA. ⁴The Ferrier Research Institute, Victoria University of Wellington; Gracefield Research Centre, Lower Hutt, 5046, New Zealand. 5Laboratory for Intravital Imaging and Dynamics of Tumor Progression, VIB Center for Cancer Biology, Leuven, 3000, Belgium. ⁶Intravital Imaging Expertise Center, VIB Center for Cancer Biology, Leuven, 3000, Belgium. ⁷Flow Cytometry Technology Platform, Faculty of Biology, Medicine and Health, University of Manchester, M13 9PT. 8Copenhagen Center for Glycomics, Department of Cellular and Molecular Medicine, Faculty of Health Sciences, University of Copenhagen, Blegdamsvej 3, DK-2200 Copenhagen N, Denmark. 9Manchester Cell-Matrix Centre, Division of Cell Matrix Biology and Regenerative Medicine, School of Biological Sciences, Faculty of Biology Medicine and Health, The University of Manchester, M13 9PT Manchester, United Kingdom. 10 Division of Biomedical and Life Sciences, Faculty of Medicine and Health, Lancaster University; Lancaster, LA1 4YG, UK. ¹¹Geoffrey Jefferson Brain Research Centre, Manchester Academic Health Science Centre, Northern Care Alliance NHS Group, University of Manchester; Manchester, M13 9PT, UK.

*Corresponding author. Email: <u>douglas.dyer@manchester.ac.uk</u> (D.P.D.); <u>a.saunders@lancaster.ac.uk</u> (A.E.S.)

Abstract

The glycocalyx is a proteoglycan-rich layer present on the surface of all mammalian cells that is particularly prevalent on endothelial cells lining the vasculature. The glycocalyx is thought to mediate leukocyte migration by masking adhesion molecules and reducing leukocyte adhesion to the endothelium. Leukocyte recruitment is a key driver of inflammatory diseases, including the chronic skin disease, psoriasis. Here, we showed

[†]These authors contributed equally to this work.

that leukocytes had heparan sulfate, an important glycocalyx component, on their cell surface, which was lost in response to psoriasis-like skin inflammation, whereas endothelial heparan sulfate was unaffected. Treatment with a heparan sulfate mimetic during psoriasis-like skin inflammation in mice protected heparan sulfate from cleavage by heparanase and resulted in reduced leukocyte accumulation in the skin. However, clinical signs of inflammation were increased because of the reduced numbers of T regulatory cells that were recruited. These findings refine our understanding of immune cell recruitment by revealing the presence and function of a heparan sulfate glycocalyx on immune cells and highlight the complex effects of heparanase inhibitors on the immune response in this context.

INTRODUCTION

During inflammatory disease, the excessive recruitment of leukocytes results in aberrant inflammation¹. The chronic inflammatory skin disease, psoriasis, is associated with the accumulation of large numbers of leukocytes in the dermis, resulting in raised, itchy, and scaly skin lesions². Despite the recruitment of immune cells into tissues being a clear driver of inflammation, there are currently no therapeutic strategies targeting leukocyte recruitment as a treatment for psoriasis³. Indeed, although studied for many years, there are still large gaps in our knowledge about the process of leukocyte migration in general⁴. Much research on leukocyte transmigration out of blood vessels has focused on endothelial cell adhesion molecules, such as selectins and immunoglobulin-like adhesion molecules⁵; however, much less attention has been paid to the molecules that initiate and

regulate the initial interactions between leukocytes and the endothelium: the proteoglycans⁶.

All mammalian cells likely express proteoglycans on their surface to varying extents as a part of the cell surface glycocalyx⁷. This layer is formed from core proteins, such as syndecans and glypicans, as well as glycosaminoglycans, such as heparan sulfate (HS)⁸. Despite glycocalyces being present on the surface of all cells, research until now has focused heavily on the glycocalyx of the vascular endothelium. Here, the glycocalyx protrudes up to 2 microns from the cell surface⁹, making it one of the first layers to come into contact with leukocytes within blood vessels, and potentially regulating early interactions between leukocytes and endothelia¹⁰. The glycocalyx also supports the functions of chemokines^{11, 12}, altering their availability to leukocytes and thereby affecting migration.

However, the glycocalyx is also thought to have anti-adhesive properties because of its shielding of endothelial cell adhesion molecules from binding by leukocytes⁹. During inflammation, the glycocalyx can be shed by factors, including shear stress¹³, reactive oxygen species¹⁴, and enzymatic degradation by enzymes such as heparanase, which cleaves HS from the glycocalyx¹⁵. This shedding of the endothelial glycocalyx has promigratory effects, which are thought to be due to the increased exposure of adhesion molecules that are masked by the glycocalyx at rest¹⁰. Glycocalyx shedding is associated with several inflammatory conditions, including sepsis¹⁶, COVID-19¹⁷, diabetes¹⁸, and psoriasis¹⁹. Compared to the growing number of studies on the role of the endothelial

glycocalyx in inflammatory diseases, very little is known about its counterpart; the leukocyte glycocalyx. Previous studies showed the presence of proteoglycans, including HS proteoglycans, on the surface of leukocytes²⁰⁻²², yet little is known about the structure of this layer or its role in the regulation of leukocyte migration.

Here, we found that a model of psoriasis-like skin inflammation in mice is not associated with endothelial HS shedding, although we could not rule out changes to the ultrastructure of the cell surface glycocalyx. However, we observed changes in the leukocyte glycocalyx, which we showed was present on the surface of skin leukocytes in vivo. Furthermore, we demonstrated that the use of the HS mimetic Tet-29 reduced immune cell recruitment into the skin, potentially through its inhibitory action on heparanase. Counterintuitively, this reduced immune cell recruitment exacerbated skin inflammation, which may be due to the reduced recruitment of regulatory T (T_{reg}) cells. Our findings highlight a previously uncharacterized mechanism for immune cell recruitment in vivo, whereby myeloid cells release heparanase and degrade HS on the surface of leukocytes, facilitating their entry into the tissue.

RESULTS

Aldara cream stimulates moderate changes in the endothelial glycocalyx

During inflammation, leukocytes are recruited into tissues by passing through the vascular endothelium²³. Therefore, we hypothesized that the endothelial glycocalyx could play a role in psoriasis-like skin inflammation by regulating immune cell recruitment. To assess this, we quantified the numbers of leukocytes in naïve skin and in psoriasis-like skin

inflammation to determine whether immune cells were recruited. Aldara cream was applied topically to the ear pinnae of mice for 6 consecutive days (Fig 1A), which led to visible erythema (redness) and scaling of the skin (Fig 1B), epidermal thickening (Fig 1C, D), and increased clinical signs of inflammation (Fig S1A, B, C) as shown previously^{24, 25}. Furthermore, Aldara cream induced the accumulation of large numbers of CD45⁺ cells into the skin, peaking at day 6 (Fig 1E), with significantly greater numbers of dendritic cells (DCs), MHCII⁺ macrophages, monocytes, neutrophils, and TCR β ⁺ T cells in Aldara-treated skin compared to those in naive skin (Fig 1F and fig. S2).

Psoriasis is associated with angiogenesis,²⁶ which may enable the increased migration of leukocytes out of blood vessels and into the skin²⁷. Similarly, Aldara cream treatment resulted in greater skin vascularization when compared to that of naïve skin (Fig S1D, E, F). To determine whether these vascular changes were accompanied by changes in the endothelial glycocalyx lining the blood vessel, we measured the amount of serum HS by ELISA. Aldara cream—treated mice had significantly greater concentrations of HS in their serum compared to that of naïve mice (Fig 1G), an indicator of glycocalyx shedding^{7,10}. To directly analyze whether Aldara-induced inflammation affected the overall structure of the endothelial glycocalyx, we performed intravital imaging of the resting and inflamed ear in live mice using the general glycocalyx marker, wheat germ agglutinin (WGA)²⁸, on endothelial (CD31⁺) vessels (Fig. 2A-C). We did not observe any changes in the intensity (Fig. 2B) or thickness (Fig. 2C) of the glycocalyx structure lining the dermal vasculature after Aldara treatment.

We next wished to specifically analyze one of the key glycocalyx components, HS, and determine whether the source of increased circulating HS was the dermal endothelial glycocalyx. To do so, we performed immunofluorescence staining of skin sections for HS together with CD31 as a marker for vascular endothelial cells (Fig 2D, E). This revealed no significant changes in the mean fluorescence intensity (MFI) of HS across blood vessels after administration of Aldara cream (Fig 2F). HS amounts were also similar on naïve and inflamed skin endothelial cells (CD45- CD31+) when examined by flow cytometry (Fig 2G, H). The specificity of the flow cytometry-based detection of HS with the 10e4 antibody was confirmed in experiments with CHO cells with and without the capacity to produce HS GAGs (Fig. S3)²⁹. In contrast, we observed an approximately 50% reduction in the amount of Syndecan-1 on the surface of endothelial cells 6 days after Aldara treatment (Fig. 2I, J). These approaches suggested that there were minimal changes in the overall endothelial glycocalyx structure in response to Aldara treatment in this context. Together, these data indicate that Aldara-induced remodeling of the endothelial glycocalyx within the mouse ear may be specific to individual components, for example, Syndecan-1, although we cannot rule out the possibility of additional ultrastructural changes to the endothelial glycocalyx structure.

Leukocytes have a cell surface glycocalyx, from which HS is lost in response to psoriasis-like skin inflammation

Previous studies suggested that human monocytes have a detectable glycocalyx^{30, 31} that can be observed by electron microscopy. More specifically, several immune cell subsets, including monocytes²⁰, neutrophils²¹ and macrophages²², may express HS on their

surface; however, little is known about the function of the leukocyte glycocalyx during inflammation in vivo. To determine whether the source of circulating HS in inflammation could be immune cells, we used both ImageStream (Fig 3A) and flow cytometry (Fig 3B) to reveal a population of HS⁺CD45⁺ cells in the blood and skin, respectively, which is reduced in size in response to psoriasis-like skin inflammation (Fig 3B, C). Uniform Manifold Approximation and Projection (UMAP) visualization of leukocytes from naïve skin showed widespread expression of HS on the surface of macrophages, monocytes, DCs, T cells, T_{reg} cells, and neutrophils (Fig 3D, E). Monocytes and neutrophils had the greatest proportion of HS+ cells, as well as the greatest decrease in HS positivity in response to psoriasis-like skin inflammation (Fig 3F). A relatively high percentage of T_{req} cells expressed HS on their surface; however, this was not significantly reduced under inflammatory conditions (Fig 3F). We also analyzed HS (Fig 3G) and Sydecan-1 (Fig 3H) on the surface of immune cells in the blood, with or without Aldara treatment, by flow cytometry, (fig. S4). This analysis confirmed the presence of HS and Syndecan-1 on the surface of immune cells at different frequencies and that they were shed in a cell-type specific manner in response to Aldara.

The only mammalian protein capable of cleaving HS along the polysaccharide chain is the endo-glucuronidase, heparanase³². We first demonstrated that heparanase protein was increased in abundance in both the blood (Fig 4A) and the skin (Fig 4B) after Aldara treatment. Flow cytometric staining for heparanase stored intracellularly in leukocytes revealed that cells of the myeloid lineage had the greatest percentage of heparanase-positive cells (Fig 4C). In particular, a proportion of monocytes showed heparanase

staining (Fig 4D), which was reduced after treatment of the skin with Aldara cream (Fig 4D, E), possibly indicating its release from the cell. We treated bone marrow cells with the main active ingredient of Aldara cream (imiquimod) alone or in combination with the cytokine interleukin-17 (IL-17) (Fig 4F). This approach confirmed the release of heparanase from immune cells in response to imiquimod either alone or in combination with IL-17, but not IL-17 alone (Fig 4F). Together, these data suggest that leukocytes have a glycocalyx on their cell surface, which is shed in response to heparanase released by immune cells (and potentially other cell types) during skin inflammation.

The HS mimetic Tet-29 lessens HS shedding from leukocytes and reduces their accumulation in the skin during psoriasis-like inflammation

To determine the importance of HS loss from the surface of leukocytes, we injected mice with the HS mimetic Tet-29 as well as treating them with Aldara cream (Fig 5A and S5). Zubkova et al.³³ showed that Tet-29 is a potent heparanase inhibitor and reduces the cleavage of a HS pentasaccharide. Here, flow cytometry revealed that Tet-29 partially protected HS on leukocytes during skin inflammation, resulting in a similar proportion of CD45⁺ cells staining positively for HS in inflamed Tet-29 treated mice as that in naïve mice (Fig 5B). Furthermore, Tet-29 treatment resulted in a reduced amount of circulating HS in the blood during inflammation compared to that in phosphate-buffered saline (PBS)-treated, control mice (Fig 5C), indicative of reduced glycocalyx shedding.

We hypothesized that protecting leukocytes from HS degradation would reduce their migration into the skin and, as a result, would lead to reduced psoriasis-like skin

inflammation. However, we found that the clinical readouts of inflammation were significantly exacerbated in mice administered Tet-29 and treated with Aldara cream relative to those in Aldara-treated mice injected with PBS as a negative control (Fig 5D). Epidermal thickness, a hallmark of psoriasis severity³⁴, which was measured by haematoxylin and eosin (H&E) staining (Fig 5E), was significantly greater in inflamed Tet-29-treated mice compared to that in inflamed control mice (Fig 5F). To investigate how inflammation was increased rather than reduced by Tet-29, we performed flow cytometry to examine the numbers of leukocytes in the skin. Counterintuitively, we found that the overall numbers of CD45⁺ cells in inflamed Tet-29-treated skin were decreased compared to those in inflamed, PBS-treated skin, but were greater than those in uninflamed skin (Fig 5G), suggesting that Tet-29 partially blocked the accumulation of immune cells in the skin in response to inflammation. MHCII+ macrophages and neutrophils were significantly reduced in number in response to Tet-29 (Fig 5H). Similar effects were seen in inflamed mice treated with a related HS mimetic³⁵, which also reduced leukocyte recruitment into the skin and exacerbated inflammation (Fig S6). These data suggest that the protection afforded by HS on the immune cell surface during psoriasis-like skin inflammation reduced the ability of leukocytes to transmigrate into the skin.

To investigate why skin inflammation is exacerbated while immune cell numbers were reduced in the skin in response to Tet-29, we examined the numbers of T_{reg} cells in the skin. T_{reg} cells are an abundant anti-inflammatory cell type in the skin, which are capable of releasing factors such as IL-10 to reduce inflammation³⁶. We found that the number of T_{reg} cells was significantly reduced during skin inflammation in Tet-29 treated mice relative

to that in control mice (Fig 5I), suggesting that the HS mimetic may reduce the ability of T_{reg} cells to enter the skin and suppress the immune response. Indeed, we found that the amount of IL-10, as measured by ELISA, was reduced in Tet-29–treated compared to that in PBS-treated inflamed skin (Fig 5J).

To confirm that the reduced accumulation of T_{reg} cells led to exacerbated inflammation in Tet-29–treated, inflamed mouse skin, we treated mice with Aldara cream and injected them with anti-CD25 antibody to deplete $T_{reg\,cell}$ numbers (Fig S7A, S7B). Depletion of T_{reg} cells significantly increased the signs of inflammation in the skin, including ear thickness, redness, and scaling (Fig 5K), epidermal thickening (Fig. 5L), and IL-17 production in the ear draining lymph node (Fig S7C).

In addition to T_{reg} cell depletion, Tet-29 treatment reduced the numbers of myeloid cells, including MHCII+ macrophages and neutrophils in the skin, as described earlier (Fig 5H). To determine the effect of neutrophil depletion, we used an anti-Ly6G antibody to deplete neutrophils in the skin of mice with psoriasis-like skin inflammation without affecting T cells (Fig S8A, B, C). However, no significant differences in inflammation were observed (Fig S8D-H), suggesting that neutrophils do not affect the clinical signs of psoriasis-like skin inflammation. Therefore, in the context of Tet-29 treatment, reduced numbers of neutrophils in the skin would likely not affect the severity of inflammation.

iCCR knockout (KO) mice, which lack the chemokine receptors CCR1, CCR22, CCR3, and CCR5^{37, 38}, had reduced numbers of myeloid cells in the skin after treatment with

Aldara cream, including DCs, monocytes, and some macrophages (Fig. S9A, S9B), but had unchanged numbers of neutrophils (Fig. S9C) and T_{reg} cells (Fig S9D). Despite this, the *iCCR* KO mice showed no differences in psoriasis-like skin inflammation severity compared to that of their littermate controls (Fig S9E-I). These findings demonstrate that the recruitment of myeloid cells into the skin does not affect the severity of psoriasis-like skin inflammation. Thus, in Tet-29–treated mice, the reduced numbers of myeloid cells are unlikely to affect the severity of inflammation. These data indicate that reduced HS shedding from the leukocyte surface in response to psoriasis-like skin inflammation decreases immune cell accumulation in the skin. This exacerbates skin inflammation because of the reduced number of T_{reg} cells in the skin and the associated reduction in anti-inflammatory cytokines.

Loss of cell surface HS results in reduced monocyte migration in vitro

To determine whether the loss of cell surface HS on leukocytes during inflammation promoted cell migration into inflamed tissues, we used bacterial heparinase as it is a robust experimental tool, to enzymatically degrade HS from the surface of murine bone marrow cells (Fig 6A, B) and investigated the ability of these cells to adhere to endothelial cells (Fig 6C, D) and migrate toward the chemokine CCL7 (Fig 6E, F). In the absence of cell surface HS, both adhesion to endothelial cells and migration of monocytes toward CCL7 were increased (Fig 6D and F). The specificity of these results to the enzymatic function of heparinase was confirmed by heat inactivation of the enzyme, resulting in reversal of these effects on adhesion (Fig S10A) and migration (Fig S10B). These data indicate that leukocytes have an increased ability to adhere to endothelial cells and

migrate when they have reduced amounts of HS on their cell surface. These observations provide a potential explanation for how the HS mimetic Tet-29 reduces the numbers of immune cells in the skin during inflammation, whereby the inhibition of HS shedding impairs the ability of immune cells to migrate from the circulation into inflamed tissues. This suggests that the reduction in leukocyte HS under inflammatory conditions may be an in vivo requirement to enable the recruitment of immune cells to the site of inflammation.

DISCUSSION

The remodeling of the glycocalyx on the endothelium and its role in facilitating leukocyte recruitment has been increasingly studied over the last 20 years, particularly in the context of inflammatory diseases^{39, 40}. Yet, little is known about the function of its counterpart, the leukocyte surface glycocalyx, and how it may be altered during inflammation. Here, we demonstrated the presence of a leukocyte glycocalyx in vivo and showed its remodeling in response to skin inflammation, suggesting a previously uncharacterized mechanism for in vivo leukocyte recruitment into the skin.

Although the breadth of glycocalyx research has expanded over time, it remains primarily focused on the endothelial glycocalyx. Li *et al.*¹⁹ demonstrated that human patients with psoriasis have reduced amounts of HS on the dermal vascular endothelium than do healthy patients; however, the leukocyte glycocalyces in these patients were not examined. This common focus on the endothelial glycocalyx has produced assumptions. For example, increased amounts of circulating glycocalyx components, such as HS and

protein cores, are assumed to indicate their shedding from the endothelial glycocalyx. Our findings of a glycocalyx on the immune cell surface challenge this assumption. We propose that the loss of HS from the leukocyte surface, in addition to the endothelial surface, may contribute to the increased circulating HS found in inflamed mice in our study. Other cell types likely also contribute to this process, including fibroblasts and keratinocytes, both of which produce HS⁴¹. These data emphasize the importance of future investigations of the cell-specific functions of HS across various cell types.

Much of the published work on heparanase-mediated degradation of the endothelial glycocalyx has focused on endothelial cells as the primary source of heparanase. Here, we showed that myeloid cells are potentially another important source of the enzyme, a finding supported by Arokiasamy *et al.*⁴² who identified macrophages as a key source of heparanase. This suggests a more widespread expression of heparanase and reveal that its' function is specific to different inflammatory contexts.

Having demonstrated the presence of an HS-containing glycocalyx on immune cells, we next examined its function. Enzymatic degradation of leukocyte HS increased the ability of the cells to migrate through a transwell (Fig 6). Sabri *et al.*⁴³ showed a similar finding, with THP1 cells shedding a proportion of their cell surface glycocalyx in response to IFN- γ , resulting in increased cell adhesion to antibody-coated spheres. Shedding the leukocyte glycocalyx may result in the increased exposure of chemokine receptors on the cell surface, enabling monocytes to bind to chemokines more readily, resulting in increased migration⁴⁴. In vivo, leukocyte glycocalyx shedding may also expose cell

surface adhesion molecules, enabling greater adhesion to endothelial cells and subsequent transmigration. However, other in vitro studies^{45, 46} showed opposing effects of HS on migration, with reduced glycosaminoglycans on the cell surface associated with their reduced ability to bind to chemokine. These data suggest that the functions of leukocyte glycocalyx shedding may be context-dependent and complex beyond simply shielding and exposing adhesion molecules.

Heparanase inhibitors have been developed to treat inflammatory diseases⁴⁷⁻⁴⁹ and cancers⁵⁰⁻⁵³. Our data support the idea that the HS mimetic, Tet-29, inhibits heparanase in vivo. Peck *et al.*⁵⁴ treated mice with Tet-29 during a model of multiple sclerosis, which resulted in reduced leukocyte recruitment into the central nervous system. Here, we expanded on those findings by providing a potential mechanism for how Tet-29 reduces leukocyte recruitment, through the protection of HS on the leukocyte surface. However, it is important to note that Tet-29 may also affect other components of the migration process, such as binding to cytokines⁵⁵, chemokines¹¹ or integrins⁵⁶.

Our findings demonstrate that heparanase inhibitors have complex effects on the immune system in this context. We hypothesize that in our model, pro-inflammatory cell recruitment is not the sole driver of inflammation, because $\chi \delta T$ cells and group 3 innate lymphoid cells, which drive the inflammation⁵⁷, are largely skin resident⁵⁸, whereas T_{reg} cells are more dependent on recruitment to the skin⁵⁹. Therefore, reducing immune cell recruitment to the skin with Tet-29 in this model only marginally affected pro-inflammatory

cell activity, but more markedly affected anti-inflammatory T_{reg} migration, resulting in the exacerbated inflammation observed here.

Based on our findings, we propose that the recruitment of monocytes into the skin during psoriasis-like skin inflammation and their release of heparanase results in the cleavage of HS, enabling subsequent immune cells to migrate into the skin more readily (Fig 7), a finding supported by previous studies⁶⁰⁻⁶⁴. Furthermore, monocytes may be able to cleave HS on their own cell surfaces, as well as on the surface of other immune cells, to facilitate their recruitment into inflamed skin. Together, these findings demonstrate the importance of HS proteoglycans in regulating leukocyte recruitment in inflammatory disease. However, they also challenge the model that these proteoglycans are primarily endothelial and emphasize the importance of HS on leukocytes themselves.

MATERIALS AND METHODS

Mice

All animal experiments were locally ethically approved and performed in accordance with the UK Home Office Animals (Scientific Procedures) Act 1986. C57BL/6 mice were obtained from Charles River Laboratories. *iCCR* KO mice and *iCCR* reporter mice, expressing different fluorescent proteins under the control of the *CCR1*, *CCR2*, *CCR3*, and *CCR5* promoters, were generated by Professor Gerard Graham (University of Glasgow, UK) on a C57BL/6N background³⁷ and were bred and maintained in specific pathogen-free conditions in house. Mice were 7- to 14-weeks old and female, except for iCCR mice which were mixed sex.

Induction of psoriasis-like skin inflammation

Psoriasis-like skin inflammation was induced as previously described²⁵. Briefly, mice were anesthetized and treated daily with 10 mg of Aldara cream (Meda Pharmaceuticals) containing 5% Imiquimod, by topical application on both ear pinnae for 6 days (days 0 to 5). Ear thickness was measured daily with a digital micrometer (Mitutoyo), and ear scaling and redness were scored daily.

Glycocalyx and immune cell modulation

To inhibit the degradation of HS, mice were injected intraperitoneally (i.p.) with 600 μg of the HS mimetic Tet-29³³ or Tri-6j³⁵, kindly provided by Dr Olga Zubkova (University of Wellington, New Zealand), or with phosphate-buffered saline (PBS) as a control, daily for 7 days (days 1 to 5) together with Aldara cream (given on days 0 to 5, as described earlier). To deplete T_{reg} cells, mice were injected i.p. with 250 μg of anti-CD25 antibody (BioXCell, clone PC-61.5.3) or with PBS as a control, on days -2, 0, 2, and 4, together with Aldara cream (given on days 0 to 5, as described earlier). To deplete neutrophils, mice were injected i.p. with 500 μg of anti-Ly6G antibody (BioXCell, clone 1A8) or with 500 μg isotype control (BioXCell), on days -2, 0, 2, and 4, together with Aldara cream (given on days 0 to 5, as described earlier).

H&E staining

Ear tissue was fixed in 10% neutral-buffered formalin (Sigma Aldrich), embedded in paraffin, and cut to 5-µm sections. H&E staining was performed with an automated

Shandon Varistain V24-4. Images were acquired with a 3D HISTECH Pannoramic-250 microscope slide-scanner (3D HISTECH). Snapshots and measurements were taken with Case Viewer software (3D HISTECH). Thickness measurements of both the epidermis and of the whole ear were taken at three different points on each section, and epidermal thickness was quantified as a percentage of the total skin thickness. At least three sections were measured per mouse, and data points represent the mean epidermal thickness per mouse.

Cell isolation

Ears were removed from euthanized mice and were split in half. The tissue was digested with 0.5 mg/ml DNAse I (Roche) and 0.25 mg/ml Liberase TM (Roche) in complete RPMI [RPMI-1640 (Sigma-Aldrich) supplemented with 10% heat-inactivated FBS (Life Technologies Ltd), 1% Penicillin-Streptomycin solution, 1 mM Sodium Pyruvate, 2 mM L-glutamine, 25 nM 2-β-mercaptoethanol, 1x non-essential amino acid solution, 20 mM HEPES buffer; (all Sigma-Aldrich)], incubated with shaking for 2 hours at 37°C, before disaggregation in a Medimachine System (BD BioSciences) for 6 min. Debris was removed by filtering through a 70-μm cell strainer before the cells were washed and counted by Trypan blue exclusion with a hemocytometer. Ear-draining (auricular) lymph nodes (LNs) were collected from mice in complete RPMI, and single-cell suspensions were acquired by gentle agitation on a 70-μm strainer. Blood samples were collected by cardiac puncture under terminal anesthesia and were placed directly into in EDTA (Lonza). Red blood cells were lysed with ammonium-chloride-potassium (ACK) lysis buffer (Gibco). Bone marrow cells were collected by centrifugation of fibulas and tibias at

15,000*g* for 15 s, and then red blood cells were lysed with ACK lysis buffer. WT and HS KO, lacking the *B4Galt7* gene that is crucial to GAG synthesis, Chinese hamster ovary (CHO) cells were maintained and cultured as described previously²⁹.

Flow cytometric analysis

Cells to be examined for cytokine production were resuspended in a stimulation medium consisting of complete RPMI (as described earlier) with 10 µM Brefeldin A, 50 ng/mL phorbol 12-myristate 13-acetate (PMA), and 500 ng/mL ionomycin (all Sigma Aldrich) and incubated for 4 hours at 37°C. Cells for flow cytometric analysis were incubated with a Live/dead blue fixable stain (Invitrogen, ThermoFisher Scientific) diluted to 1:2000 with PBS and Fc block (see table S1) and then stained with extracellular antibodies (table S1) in FACS wash (PBS, 1% FBS, 2 mM EDTA). Cells were fixed with the Foxp3/transcription factor staining buffer set (eBioscience) for 15 min. Where indicated, overnight staining with a biotinylated anti-HS antibody (table S1) followed by a secondary fluorescently labelled streptavidin conjugate (table S1) was performed. Where intracellular staining was performed, cells were permeabilized with the Foxp3/transcription factor staining buffer set (eBioscience), and cells were incubated for 2 hours with intracellular antibodies (table S1) in permeabilization buffer (eBioscience). Where appropriate, cells were also stained with an anti-rabbit IgG to detect the anti-heparanase antibody (table S1). Data were acquired with a Fortessa X20 (Becton Dickinson) flow cytometer with BD FACSDiva Software. Data were analyzed with FlowJo software (version 10.8.0) (Treestar Inc.) Gating of cells was performed according to the gating strategies in figs. S2 or S4.

UMAP clustering

UMAP plots were generated with R^{64} by clustering cells based on expression of the markers CD11b, CD11c, CD3, F4/80, Foxp3, Ly6C, Ly6G, MHCII, TCR β , and TCR $\gamma\delta$.

ELISA

Skin samples were snap-frozen before undergoing bead beating with a TissueLyser II (Qiagen) at 20 Hz for 2 min with a 5-mm ball bearing in a 2-ml tube. Tissue was then placed in lysis buffer [0.1% Triton X100 (Sigma-Aldrich)] with cOmplete mini protease inhibitors (Roche, 1 tablet per 10 ml of lysis buffer) in PBS for 30 min at 4°C. Blood samples were taken from mice by cardiac puncture under terminal anesthesia and left on ice to coagulate for 4 hours. Blood was centrifuged at 15,000*g* for 10 min at 4°C, and supernatants were collected and frozen. The amounts of heparanase and IL-10 were measured with ELISA kits from Finetest and R&D systems, respectively. Data depict the mean of duplicates for each sample.

Intravital imaging

Alexa Fluor 594–conjugated anti-CD31 conjugated (clone: MEC13.3, Biolegend Cat. No.: 102520) was co-injected i.p. at 15 μg/mouse with Alexa Fluor 633–conjugated WGA (ThermoFisher Scientific Cat. No.: W21404) at 6.5 mg/kg. Thirty minutes after injection, mice were anesthetized with isoflurane and kept at 32°C by a climate chamber surrounding the entire stage of the microscope including the objectives. Mice were imaged non-invasively through the depilated ear papillae on an inverted Leica SP8 Dive system (Leica Microsystems, Mannheim, Germany) equipped with three tunable HyD-

RLD detectors and an InSight X3 laser (Spectra-Physics) using the Leica Application Suite X (LasX) software. All images were collected at 12 bit and acquired with a 25x water immersion objective with a free working distance of 2.4 mm (HC FLUOTAR L 25x/0.95 W VISIR 0.17). Imaging was performed at a frequency of 600 Hz and bi-directional scanning, with a two-photon wavelength of 780 nm. Using the tunable bandpass filters, the second harmonic generation (SHG, collagen I) was detected at 380 – 400 nm, the CD31-AF594 between 580 and 620 nm, and the WGA-AF633 at 640 to 700 nm. Regions of interest (ROIs) were identified in overview merged tile images, and individual Z-stacks were acquired at a step size of 2 µm. Maximum projections and subsequent intensity analysis of vascular wall signal ROIs with four per image, and three to six images per mouse were quantified with ImageJ software. The WGA signal was finally normalized to the detected CD31 intensity. Maximum projections and WGA signal thickness were assessed by measuring the vessel wall thickness with ImageJ with four per image, and three to six images per mouse were quantified with ImageJ. This was done for ROIs with the most prominent (thickest) WGA signal of a single vessel or branch.

Immunofluorescence staining

Ear tissue was fixed in 10% neutral-buffered formalin (Sigma Aldrich) and then embedded in paraffin and cut to form 5-µm sections. The sections were dewaxed in xylene and rehydrated in decreasing concentrations of ethanol. Antigen retrieval was performed by boiling in Tris-EDTA buffer (pH 9.0) before permeabilization in 0.5% Triton-X100 (Sigma-Aldrich). Sections were blocked with 2% donkey serum (Sigma) and 1% BSA in TBS for 30 min at room temperature, and then treated with an Avidin/Biotin blocking kit (Vector)

according to the manufacturer's instructions. Sections were further blocked with Mouse Ig Blocking Reagent (Mouse on Mouse Immunodetection Kit, Vector) for 1 hour. Sections were incubated with primary antibodies (table S2) overnight at 4°C, followed by anti-HS antibody (table S2) for 10 min, followed by tertiary antibodies against HS and secondary antibodies against CD31 (table S2) for 1 hour at room temperature, all of which were made up in MOM diluent (Mouse on Mouse Immunodetection Kit, Vector). Nuclei were visualized with DAPI (49,6-diamidino-2-phenylindole, Thermofisher) staining (0.2 µg/ml for 5 min), and sections were mounted with Prolong Gold antifade mountant (Thermofisher). Images were collected on a Zeiss Axioimager.D2 upright microscope using 10x, 20x, 40x, and 63x EC Plan-neofluar objective lenses and captured with a Coolsnap HQ2 camera (Photometrics) through Micromanager software v1.4.23. Images were processed and analyzed with ImageJ software (version 1.53a).

Immunofluorescence image analysis

HS abundance was quantified in images by selecting endothelial cells (based on the expression of CD31) on the perimeter of blood vessels excluding the lumen, and measuring the mean fluorescence value for HS staining within these areas. At least three vessels were measured per section and at least three sections were measured per mouse. Data represent the MFI per mouse. Vascularization of the skin was quantified by measuring the number of pixels staining positively for CD31 and dividing this by the number of pixels within the boundary of the skin section. At least five sections were measured per mouse.

ImageStream analysis

Blood cells were stained and fixed as described earlier in ImageStream buffer (PBS containing 1% FCS). Data acquisition was performed on an ImageStreamX (Amnis Mk-II) equipped with 405-, 488-, 561-, and 642-nm lasers. Single cells were discriminated from cell aggregates based on area and aspect ratio. In-focus cells were selected based on the high-gradient RMS of the bright field image. Images of cells were acquired with a ×40 objective, including bright-field images (channels 1 and 9; 435 to 480 nm and 570 to 595 nm), HS and SA (PE-CF594 AMS Biotechnology and BioLegend, respectively; channel 4; 595 to 642 nm), CD45 (BV510, BioLegend; channel 8; 505 to 570 nm), Ly6C (APC, BioLegend; channel 11; 642 to 745 nm). All antibodies were used at a 1:100 dilution. All data analysis was performed with IDEAS software version 6.3.

In vitro heparinase treatment

Bone marrow cells were collected by centrifugation of fibulas and tibias at 15,000g for 15 s, and then red blood cells were lysed with ACK lysis buffer. Cells were resuspended at 2.5×10^6 cells/ml and treated with heparinase I and III (1 U/ml) from *Flavobacterium heparinum* (Sigma-Aldrich) for 6 hours at 37°C in complete RPMI. Controls were included for each experiment whereby heparanase was heat-inactivated at 100°C for 5 min.

Adhesion assays

Two days before the assays, murine endothelial cells (B.End.5 cells, kindly provided by Professor Catherine Lawrence, University of Manchester) were seeded in a clear fibronectin-coated 96-well plate at 10,000 cells/well. Before use, endothelial cells were

stimulated with 360 ng/mL IL-1 β for 4 hours at 37°C. Bone marrow cells from iCCR reporter mice were collected and treated with heparinase (as described earlier) or with medium as a control, before stimulation with 100 ng/ml CCL7 for 30 min at 37°C. Endothelial cells were washed in medium before leukocytes in CCL7-containing medium were added to the wells and co-cultured on endothelial cell monolayers for 30 min at 37°C. Non-bound cells were aspirated and the fluorescence in the wells was promptly measured on a plate reader (FlexStation 3, Molecular Devices, 505-nm excitation, 515-nm emission) to determine the extent of leukocyte adhesion for each condition.

Migration experiments

Migration assays were performed with 24-well transwell plates with 5-μm pore size filter inserts (Corning). CCL7 was added at a final concentration of 100 nM in the bottom well in complete RPMI. One hundred microliters of bone marrow containing 1.25 x 10⁷ cells was added to the upper chamber and the cells were allowed to migrate for 2 hours at 37°C. The migrated cells were then collected and analyzed by flow cytometry. The proportion of cells that had migrated was calculated by dividing the number of migrated cells by the number of cells recovered from a well with no transwell insert. Data are from two independent experiments, each performed in triplicate.

Statistical analysis

All data were analyzed with GraphPad Prism 10. Data were tested for normality with a Shapiro-Wilks test. Unpaired *t* tests (for two groups) or one-way ANOVA with Tukey's multiple comparison test (for more than two groups) were used for parametric data. Non-

parametric data were analyzed by Mann-Whitney U tests (for two groups) or Kruskal Wallis with Dunn's multiple comparisons test (for more than two groups). Data annotated as "fold-change" were normalized as a percentage of the average value of the PBS control group in each experiment.

Supplementary Materials

Figs S1 to S10. Tables S1 and S2.

References and Notes

- 1. NOURSHARGH, S. & ALON, R. 2014. Leukocyte migration into inflamed tissues. Immunity, 41, 694-707.
- 2. HAWKES, J. E., CHAN, T. C. & KRUEGER, J. G. 2017. Psoriasis pathogenesis and the development of novel targeted immune therapies. J Allergy Clin Immunol, 140, 645-653.
- 3. LANDECK, L., SABAT, R., GHORESCHI, K., MAN, X. Y., FUHRMEISTER, K., GONZALEZ-MARTINEZ, E. & ASADULLAH, K. 2021. Immunotherapy in psoriasis. Immunotherapy, 13, 605-619.
- 4. KRÜGER-GENGE, A., BLOCKI, A., FRANKE, R. P. & JUNG, F. 2019. Vascular Endothelial Cell Biology: An Update. Int J Mol Sci, 20.
- 5. SCHIMMEL, L., HEEMSKERK, N. & VAN BUUL, J. D. 2017. Leukocyte transendothelial migration: A local affair. Small GTPases, 8, 1-15.
- 6. GRAY, A. L., PUN, N., RIDLEY, A. J. L. & DYER, D. P. 2022. Role of extracellular matrix proteoglycans in immune cell recruitment. Int J Exp Pathol, 103, 34-43.
- 7. SUTHERLAND, T. E., DYER, D. P. & ALLEN, J. E. 2023. The extracellular matrix and the immune system: A mutually dependent relationship. Science, 379, eabp8964.
- 8. IOZZO, R. V. & SCHAEFER, L. 2015. Proteoglycan form and function: A comprehensive nomenclature of proteoglycans. Matrix Biol, 42, 11-55.
- 9. REITSMA, S., SLAAF, D. W., VINK, H., VAN ZANDVOORT, M. A. & OUDE EGBRINK, M. G. 2007. The endothelial glycocalyx: composition, functions, and visualization. Pflugers Arch, 454, 345-59.
- 10. MARKI, A., ESKO, J. D., PRIES, A. R. & LEY, K. 2015. Role of the endothelial surface layer in neutrophil recruitment. J Leukoc Biol, 98, 503-15.
- 11. GRAY, A. L., KARLSSON, R., ROBERTS, A. R. E., RIDLEY, A. J. L., PUN, N., KHAN, B., LAWLESS, C., LUÍS, R., SZPAKOWSKA, M., CHEVIGNÉ, A., HUGHES, C. E., MEDINA-RUIZ, L., BIRCHENOUGH, H. L., MULHOLLAND, I. Z., SALANGA, C. L., YATES, E. A., TURNBULL, J. E., HANDEL, T. M., GRAHAM, G. J., JOWITT, T. A., SCHIESSL, I., RICHTER, R. P., MILLER, R. L. & DYER, D. P. 2023. Chemokine CXCL4 interactions with extracellular matrix proteoglycans mediate widespread immune cell recruitment independent of chemokine receptors. Cell Rep, 42, 111930.

- 12. RIDLEY, A. J. L., OU, Y., KARLSSON, R., PUN, N., BIRCHENOUGH, H. L., MULHOLLAND, I. Z., BIRCH, M. L., MACDONALD, A. S., JOWITT, T. A., LAWLESS, C., MILLER, R. L. & DYER, D. P. 2023. Chemokines form complex signals during inflammation and disease that can be decoded by extracellular matrix proteoglycans. Sci Signal, 16, eadf2537.
- 13. LUPU, F., KINASEWITZ, G. & DORMER, K. 2020. The role of endothelial shear stress on haemodynamics, inflammation, coagulation and glycocalyx during sepsis. J Cell Mol Med, 24, 12258-12271.
- 14. SINGH, A., RAMNATH, R. D., FOSTER, R. R., WYLIE, E. C., FRIDÉN, V., DASGUPTA, I., HARALDSSON, B., WELSH, G. I., MATHIESON, P. W. & SATCHELL, S. C. 2013. Reactive oxygen species modulate the barrier function of the human glomerular endothelial glycocalyx. PLoS One, 8, e55852.
- 15. MASOLA, V., GRECO, N., GAMBARO, G., FRANCHI, M. & ONISTO, M. 2022. Heparanase as active player in endothelial glycocalyx remodeling. Matrix Biol Plus, 13, 100097.
- 16. SCHMIDT, E. P., YANG, Y., JANSSEN, W. J., GANDJEVA, A., PEREZ, M. J., BARTHEL, L., ZEMANS, R. L., BOWMAN, J. C., KOYANAGI, D. E., YUNT, Z. X., SMITH, L. P., CHENG, S. S., OVERDIER, K. H., THOMPSON, K. R., GERACI, M. W., DOUGLAS, I. S., PEARSE, D. B. & TUDER, R. M. 2012. The pulmonary endothelial glycocalyx regulates neutrophil adhesion and lung injury during experimental sepsis. Nat Med, 18, 1217-23.
- 17. YAMAOKA-TOJO, M. 2020. Vascular Endothelial Glycocalyx Damage in COVID-19. Int J Mol Sci, 21.
- 18. PERRIN, R. M., HARPER, S. J. & BATES, D. O. 2007. A role for the endothelial glycocalyx in regulating microvascular permeability in diabetes mellitus. Cell Biochem Biophys, 49, 65-72.
- 19. LI, Q., SHAO, S., ZHU, Z., CHEN, J., HAO, J., BAI, Y., LI, B., DANG, E. & WANG, G. 2023. An IGFBP7hi endothelial cell subset drives T cell extravasation in psoriasis via endothelial glycocalyx degradation. J Clin Invest, 133.
- 20. DEN DEKKER, E., GREFTE, S., HUIJS, T., TEN DAM, G. B., VERSTEEG, E. M., VAN DEN BERK, L. C., BLADERGROEN, B. A., VAN KUPPEVELT, T. H., FIGDOR, C. G. & TORENSMA, R. 2008. Monocyte cell surface glycosaminoglycans positively modulate IL-4-induced differentiation toward dendritic cells. J Immunol, 180, 3680-8.
- 21 CAMPBELL, E. J. & OWEN, C. A. 2007. The sulfate groups of chondroitin sulfate- and heparan sulfate-containing proteoglycans in neutrophil plasma membranes are novel binding sites for human leukocyte elastase and cathepsin G. J Biol Chem, 282, 14645-54.
- 22 EBSTEIN, S. Y., RAFIQUE, A., ZHOU, Y., KRASCO, A., MONTALVO-ORTIZ, W., YU, L., CUSTODIO, L., ADAM, R. C., BLOCH, N., LEE, K., ADEWALE, F., VERGATA, D., LUZ, A., COQUERY, S., DANIEL, B., ULLMAN, E., FRANKLIN, M. C., HERMANN, A., HUANG, T., OLSON, W., DAVIS, S., MURPHY, A. J., SLEEMAN, M. A., WEI, J. & SKOKOS, D. 2023. VSIG4 interaction with heparan sulfates inhibits VSIG4-complement binding. Glycobiology, 33, 591-604.
- 23. SUN, H., HU, L. & FAN, Z. 2021. β2 integrin activation and signal transduction in leukocyte recruitment. *Am J Physiol Cell Physiol*, 321, C308-c316.

- 24. VAN DER FITS, L., MOURITS, S., VOERMAN, J. S., KANT, M., BOON, L., LAMAN, J. D., CORNELISSEN, F., MUS, A. M., FLORENCIA, E., PRENS, E. P. & LUBBERTS, E. 2009. Imiquimod-induced psoriasis-like skin inflammation in mice is mediated via the IL-23/IL-17 axis. J Immunol, 182, 5836-45.
- 25. LINLEY, H., OGDEN, A., JAIGIRDAR, S., BUCKINGHAM, L., COX, J., PRIESTLEY, M. & SAUNDERS, A. 2023. CD200R1 promotes interleukin-17 production by group 3 innate lymphoid cells by enhancing signal transducer and activator of transcription 3 activation. Mucosal Immunol, 16, 167-179.
- 26. HAN, D., LI, F., ZHAO, Y., WANG, B., WANG, J., LIU, B., MOU, K., MENG, L., ZHENG, Y., LU, S., ZHU, W. & ZHOU, Y. 2024. IL-21 promoting angiogenesis contributes to the development of psoriasis. Faseb j, 38, e23375.
- 27. HEIDENREICH, R., RÖCKEN, M. & GHORESCHI, K. 2009. Angiogenesis drives psoriasis pathogenesis. Int J Exp Pathol, 90, 232-48.
- 28. GRAY, A., SCHIESSL, I. & DYER, D. 2023. Chronic cranial window implantation for high-resolution intravital imaging of the endothelial glycocalyx in mouse cortex. *STAR Protoc.* 4, 102712.
- 29. KARLSSON, R., PRADEEP CHOPRA, A.J., ZHANG, Y., VAKHRUSHEV, S.Y., MANDEL CLAUSEN, T., PAINTER, C.D., et al. Dissecting Structure-Function of 3-O-Sulfated Heparin and Engineered Heparan Sulfates. Science Advances 7, 52.
- 30. POLLER, W. C., LÖWA, N., SCHLEICHER, M., MÜNSTER-WANDOWSKI, A., TAUPITZ, M., STANGL, M., LUDWIG, A., WIEKHORST, F. Initial Interaction of Citrate-Coated Iron Oxide Nanoparticles with the Glycocalyx of THP-1 Monocytes Assessed by Real-Time Magnetic Particle Spectroscopy and Electron Microscopy. Scientific Reports 10, 1, 3591.
- 31. TWAMLEY, S. G., STACH, A., HEILMANN, H., SÖHL-KIELCZYNSKI, B., STANGL, V., LUDWIG, A., MÜNSTER-WANDOWSKI, A. Immuno-Electron and Confocal Laser Scanning Microscopy of the Glycocalyx. Biology 10, 5.
- 32. VLODAVSKY, I., ILAN, N. & SANDERSON, R. D. 2020. Forty Years of Basic and Translational Heparanase Research. *Adv Exp Med Biol*, 1221, 3-59.
- 33. ZUBKOVA, O. V., AHMED, Y. A., GUIMOND, S. E., NOBLE, S. L., MILLER, J. H., ALFRED SMITH, R. A., NURCOMBE, V., TYLER, P. C., WEISSMANN, M., VLODAVSKY, I. & TURNBULL, J. E. 2018. Dendrimer Heparan Sulfate Glycomimetics: Potent Heparanase Inhibitors for Anticancer Therapy. *ACS Chem Biol*, 13, 3236-3242.
- 34. GANGWAR, R. S., GUDJONSSON, J. E. & WARD, N. L. 2022. Mouse Models of Psoriasis: A Comprehensive Review. J Invest Dermatol, 142, 884-897.
- 35. SPIJKERS-SHAW, S., CAMPBELL, K., SHIELDS, N. J., MILLER, J. H., RENDLE, P. M., JIAO, W., YOUNG, S. L. & ZUBKOVA, O. V. 2022. Synthesis of Novel Glycolipid Mimetics of Heparan Sulfate and Their Application in Colorectal Cancer Treatment in a Mouse Model. Chem Asian J, 17, e202200228.
- 36. RUBTSOV, Y. P., RASMUSSEN, J. P., CHI, E. Y., FONTENOT, J., CASTELLI, L., YE, X., TREUTING, P., SIEWE, L., ROERS, A., HENDERSON, W. R., JR., MULLER, W. & RUDENSKY, A. Y. 2008. Regulatory T cell-derived interleukin-10 limits inflammation at environmental interfaces. Immunity, 28, 546-58.
- 37. DYER, D. P., MEDINA-RUIZ, L., BARTOLINI, R., SCHUETTE, F., HUGHES, C. E., PALLAS, K., VIDLER, F., MACLEOD, M. K. L., KELLY, C. J., LEE, K. M., HANSELL, C.

- A. H. & GRAHAM, G. J. 2019. Chemokine Receptor Redundancy and Specificity Are Context Dependent. Immunity, 50, 378-389.e5.
- 38. PUN, N., CYTLAK, U. M., LEE, D., DOMINGUES, R.G., CHEADLE, E., FORSTER, D., WILLIAMS, K. J., et al. CCR2-Driven Monocyte Recruitment Is Protective against Radiotherapy-Induced Intestinal Toxicity. bioRxiv.
- 39. KOLÁŘOVÁ, H., AMBRŮZOVÁ, B., SVIHÁLKOVÁ ŠINDLEROVÁ, L., KLINKE, A. & KUBALA, L. 2014. Modulation of endothelial glycocalyx structure under inflammatory conditions. *Mediators Inflamm*, 2014, 694312.
- 40. SHI, S., SUH, R., SHON, D., GARCIA, F., BUFF, J., ATKINA, M., LI, L., SUN, B., LUO, J., TO, N., CHEUNG, T., MCNERNEY, W., HEIMAN, M., BERTOZZI, C. & WYSS-CORAY, T. Glycocalyx dysregulation impairs blood-brain barrier in ageing and disease. 2025. *Nature.*
- 41. SMITH, M. M. & MELROSE, J. 2015. Proteoglycans in Normal and Healing Skin. Adv Wound Care (New Rochelle), 4, 152-173.
- 42. AROKIASAMY, S., KING, R., BOULAGHRASSE, H., POSTON, R. N., NOURSHARGH, S., WANG, W. & VOISIN, M. B. 2019. Heparanase-Dependent Remodeling of Initial Lymphatic Glycocalyx Regulates Tissue-Fluid Drainage During Acute Inflammation in vivo. Front Immunol, 10, 2316.
- 43. SABRI, S., SOLER, M., FOA, C., PIERRES, A., BENOLIEL, A. & BONGRAND, P. 2000. Glycocalyx modulation is a physiological means of regulating cell adhesion. J Cell Sci, 113 (Pt 9), 1589-600.
- 44. Jørgensen, A., Probst Brandum, E., Mikkelsen, J., Orfin, K., Boilesen, D., Egerod, K., Moussouras, N., et al. 'The C-Terminal Peptide of CCL21 Drastically Augments CCL21 Activity through the Dendritic Cell Lymph Node Homing Receptor CCR7 by Interaction with the Receptor N-Terminus'. *Cellular and Molecular Life Sciences*: CMLS 78, no. 21–22 (November 2021): 6963–78.
- 45. GOLDBLATT, J., LAWRENSON, R. A., MUIR, L., DATTANI, S., HOFFLAND, A., TSUCHIYA, T., KANEGASAKI, S., SRISKANDAN, S. & PEASE, J. E. 2019. A Requirement for Neutrophil Glycosaminoglycans in Chemokine:Receptor Interactions Is Revealed by the Streptococcal Protease SpyCEP. J Immunol, 202, 3246-3255.
- 46. SALANGA, C. L., DYER, D. P., KISELAR, J. G., GUPTA, S., CHANCE, M. R. & HANDEL, T. M. 2014. Multiple glycosaminoglycan-binding epitopes of monocyte chemoattractant protein-3/CCL7 enable it to function as a non-oligomerizing chemokine. J Biol Chem, 289, 14896-912.
- 47. ABASSI, Z., HAMOUD, S., HASSAN, A., KHAMAYSI, I., NATIV, O., HEYMAN, S. N., MUHAMMAD, R. S., ILAN, N., SINGH, P., HAMMOND, E., ZAZA, G., LUPO, A., ONISTO, M., BELLIN, G., MASOLA, V., VLODAVSKY, I. & GAMBARO, G. 2017. Involvement of heparanase in the pathogenesis of acute kidney injury: nephroprotective effect of PG545. *Oncotarget*, 8, 34191-34204.
- 48. CHEN, S., HE, Y., HU, Z., LU, S., YIN, X., MA, X., LV, C. & JIN, G. 2017. Heparanase Mediates Intestinal Inflammation and Injury in a Mouse Model of Sepsis. *J Histochem Cytochem*, 65, 241-249.
- 49. GAMEZ, M., ELHEGNI, H. E., FAWAZ, S., HO, K. H., CAMPBELL, N. W., COPLAND, D. A., ONIONS, K. L., BUTLER, M. J., WASSON, E. J., CROMPTON, M., RAMNATH, R. D., QIU, Y., YAMAGUCHI, Y., ARKILL, K. P., BATES, D. O., TURNBULL, J. E., ZUBKOVA, O. V., WELSH, G. I., ATAN, D., SATCHELL, S. C. & FOSTER, R. R. 2024. Heparanase

- inhibition as a systemic approach to protect the endothelial glycocalyx and prevent microvascular complications in diabetes. *Cardiovasc Diabetol*, 23, 50.
- 50. BARASH, U., RANGAPPA, S., MOHAN, C. D., VISHWANATH, D., BOYANGO, I., BASAPPA, B., VLODAVSKY, I. & RANGAPPA, K. S. 2021. New Heparanase-Inhibiting Triazolo-Thiadiazoles Attenuate Primary Tumor Growth and Metastasis. *Cancers (Basel)*, 13.
- 51. DE BOER, C., ARMSTRONG, Z., LIT, V. A. J., BARASH, U., RUIJGROK, G., BOYANGO, I., WEITZENBERG, M. M., SCHRODER, S. P., SARRIS, A. J. C., MEEUWENOORD, N. J., BULE, P., KAYAL, Y., ILAN, N., CODEE, J. D. C., VLODAVSKY, I., OVERKLEEFT, H. S., DAVIES, G. J. & WU, L. 2022. Mechanism-based heparanase inhibitors reduce cancer metastasis in vivo. *Proc Natl Acad Sci U S A,* 119, e2203167119. 52. SINGH, P., BLATT, A., FELD, S., ZOHAR, Y., SAADI, E., BARKI-HARRINGTON, L., HAMMOND, E., ILAN, N., VLODAVSKY, I., CHOWERS, Y. & HALF, E. 2017. The Heparanase Inhibitor PG545 Attenuates Colon Cancer Initiation and Growth, Associating with Increased p21 Expression. *Neoplasia,* 19, 175-184.
- 53. WEISSMANN, M., ARVATZ, G., HOROWITZ, N., FELD, S., NARODITSKY, I., ZHANG, Y., NG, M., HAMMOND, E., NEVO, E., VLODAVSKY, I. & ILAN, N. 2016. Heparanase-neutralizing antibodies attenuate lymphoma tumor growth and metastasis. *Proc Natl Acad Sci U S A*, 113, 704-9.
- 54. PECK, T., DAVIS, C., LENIHAN-GEELS, G., GRIFFITHS, M., SPIJKERS-SHAW, S., ZUBKOVA, O. V. & LA FLAMME, A. C. 2023. The novel HS-mimetic, Tet-29, regulates immune cell trafficking across barriers of the CNS during inflammation. *J Neuroinflammation*, 20, 251.
- 55. XIE, M. & LI, J. P. 2019. Heparan sulfate proteoglycan A common receptor for diverse cytokines. *Cell Signal*, 54, 115-121.
- 56. HASSAN, N., GREVE, B., ESPINOZA-SÁNCHEZ, N. A. & GÖTTE, M. 2021. Cell-surface heparan sulfate proteoglycans as multifunctional integrators of signaling in cancer. *Cell Signal*, 77, 109822.
- 57. PANTELYUSHIN, S., HAAK, S., INGOLD, B., KULIG, P., HEPPNER, F. L., NAVARINI, A. A. & BECHER, B. 2012. Roryt+ innate lymphocytes and $\gamma\delta$ T cells initiate psoriasiform plaque formation in mice. J Clin Invest, 122, 2252-6.
- 58. DUTTON, E. E., GAJDASIK, D. W., WILLIS, C., FIANCETTE, R., BISHOP, E. L., CAMELO, A., SLEEMAN, M. A., COCCIA, M., DIDIERLAURENT, A. M., TOMURA, M., PILATAXI, F., MOREHOUSE, C. A., CARLESSO, G. & WITHERS, D. R. 2019. Peripheral lymph nodes contain migratory and resident innate lymphoid cell populations. Sci Immunol, 4.
- 59. NORMAN, M. U., CHOW, Z., SNELGROVE, S. L., PRAKONGTHAM, P. & HICKEY, M. J. 2021. Dynamic Regulation of the Molecular Mechanisms of Regulatory T Cell Migration in Inflamed Skin. Front Immunol, 12, 655499.
- 60. POON, I. K., GOODALL, K. J., PHIPPS, S., CHOW, J. D., PAGLER, E. B., ANDREWS, D. M., CONLAN, C. L., RYAN, G. F., WHITE, J. A., WONG, M. K., HORAN, C., MATTHAEI, K. I., SMYTH, M. J. & HULETT, M. D. 2014. Mice deficient in heparanase exhibit impaired dendritic cell migration and reduced airway inflammation. Eur J Immunol, 44, 1016-30.
- 61. PUTZ, E. M., MAYFOSH, A. J., KOS, K., BARKAUSKAS, D. S., NAKAMURA, K., TOWN, L., GOODALL, K. J., YEE, D. Y., POON, I. K., BASCHUK, N., SOUZA-FONSECA-

- GUIMARAES, F., HULETT, M. D. & SMYTH, M. J. 2017. NK cell heparanase controls tumor invasion and immune surveillance. J Clin Invest, 127, 2777-2788
- 62. SASAKI, N., HIGASHI, N., TAKA, T., NAKAJIMA, M. & IRIMURA, T. 2004. Cell surface localization of heparanase on macrophages regulates degradation of extracellular matrix heparan sulfate. J Immunol, 172, 3830-5.
- 63. MAYFOSH, A. J., GOODALL, K. J., NGUYEN, T., BASCHUK, N. & HULETT, M. D. 2022. Heparanase is a regulator of natural killer cell activation and cytotoxicity. J Leukoc Biol, 111, 1211-1224.
- 64. MCINNES, L., HEALY, J., MELVILLE, J. 2018. UMAP: Uniform Manifold Approximation and Projection for Dimension Reduction. arXiv:1802.03426.

Acknowledgments: The authors acknowledge members of the Saunders lab and the Dyer lab for critical discussion. We acknowledge members of the biological services, flow cytometry, histology, and bioimaging facilities at the University of Manchester. We acknowledge the gift of ICCR KO mice from G. Graham (University of Glasgow) and endothelial cells from C. Lawrence (University of Manchester). O.Z. thanks A. Lewis and Y. Lu for an exceptional NMR and mass spectroscopy service, and Y. Li for assistance with the synthesis of HS mimetics. Diagrams created using Biorender.com. Funding: This work was funded by a Sir Henry Dale fellowship jointly funded by the Wellcome Trust and Royal Society 218570/Z/19/Z (to D.D.), a Wellcome Trust center grant 203128/A/16/Z (to D.D.), the Wellcome Trust Discovery Research platform 226804/Z/22/Z (to D.D. and H.D.S.), a Sir Henry Dale fellowship jointly funded by the Wellcome Trust and Royal Society 109375/Z/15/Z (to A.S.), the New Zealand Ministry of Business, Innovation and Employment RTVU1801 (to O.Z.), the New Zealand Breast Cancer Foundation R1703 (to O.Z.), a Wellcome Trust Immunomatrix in Complex Disease (ICD) PhD studentship 218491/Z/19/Z (to M.P.), and a Novo Nordisk Foundation grant NNF22OC0073736 (to R.L.M.). Author contributions: Conceptualization: M.P., D.D., and A.S. Methodology: M.P., I.M., R.L.M., A.S., and D.D. Investigation: M.P., A.H., I.M., J.C.M., A.J.R., H.D.S., M.N., A.S., and D.D. Visualization: M.P. Resources: O.Z., S.S.S., and R.L.M. Funding acquisition: D.D. and A.S. Project administration: D.D. and A.S. Supervision: D.D. and A.S. Writing – original draft: M.P. Writing – review & editing: M.P., D.D., A.S., and S.S.S.. Competing interests: The authors declare that they have no competing interests. Data and materials availability: All data needed to evaluate the conclusions in the paper are present in the paper or the Supplementary Materials.

Fig. 1. Topical application of Aldara cream stimulates immune cell accumulation in the skin and increases serum HS abundance. (A to G) Mice were treated with topical application of 10 mg Aldara cream to each ear pinnae daily for 0 to 6 days (A) to induce skin inflammation (B). (C) Skin was sectioned and stained with H&E. The black box highlights the magnified region. Black arrows indicate leukocytes; the yellow line shows the epidermis. Scale bars: 100 μm (left and middle); 25 μm (right).(D) Epidermal thickness was measured from images and calculated as a percentage of the total ear thickness. (E and F) The numbers of CD45⁺ cells (normalized to the mean of the untreated controls) (E) and the numbers of DCs, macrophages, monocytes, neutrophils, and T cells (F) were quantified on day 6 of Aldara treatment in both ears by flow cytometry. (G) Circulating HS in the blood was measured by ELISA and normalized to that of the untreated control (G). Each data point represents one mouse with at least three biological replicates for all panels. Data were analyzed by unpaired t test (D and G), by one-way ANOVA with Tukey's multiple comparisons test (E), and by Two-way ANOVA with Tukey's multiple comparisons test (F). Error bars represent means ± SD.

Fig. 2. The endothelial glycocalyx is changed in response to psoriasis-like skin inflammation. (A to J) Mice were treated with daily topical application of Aldara cream for 0, 1, 2, 3, or 6 days on both ear pinnae. (A) Mice were injected intravenously with anti-CD31 (pink) and WGA (green), and intravital imaging was performed on the ear skin vasculature. (B and C) Intensity analysis was performed for CD31 and WGA staining, and WGA signal was normalized to the detected CD31 intensity (B), and the thickness of the WGA layer was measured (C). (D to F) Aldara-treated mice were culled, and the skin was

stained for HS (green), CD31 (red), and DAPI (blue) (D and E). (F) The MFI of HS staining within the vessel was measured with ImageJ software. (G and H) HS expression on endothelial cells (CD45⁻CD31⁺) was measured by flow cytometry (G), and the geometric mean fluorescence intensity (gMFI) of HS on the cells was calculated (H). (I and J) Syndecan-1 expression on endothelial cells (CD45⁻CD31⁺) was measured by flow cytometry (I), and the gMFI of Syndecan-1 on the cells was calculated (J). Each data point represents one mouse, with at least three biological repeats for all panels. Scale bars for (A), (D), and (E): 50 μ m (large images) and 10 μ m (small images). Data were analyzed by one-way ANOVA with Tukey's multiple comparison test, except for the data in (B), which were analyzed by an unpaired t test. ns, not significant. Error bars represent means \pm SD.

Fig. 3. Immune cells lose cell surface HS in response to psoriasis-like skin inflammation. (A) Blood was collected from naïve mice, stained for CD45 (blue), HS (red), and Ly6C (green) and imaged with an ImageStream analyzer. (B and C) Mice were left untreated or were treated topically with Aldara cream to the ear pinnae for 6 days. HS expression on immune cells was measured by flow cytometry (B), and the percentage of total CD45⁺ cells expressing HS was quantified in both untreated and Aldara-treated skin (C). (D to F) Cells from naïve mouse skin were stained for flow cytometric analysis, and major immune cell types were clustered using the UMAP algorithm (D). (E) Cells positive for HS were mapped onto the resulting clusters. (F) The percentages of leukocyte subsets expressing HS with and without Aldara cream treatment. (G and H) Blood was collected from naïve and Aldara-treated mice and the relative abundances of HS (G) and Sdc1 (H)

were measured on immune cell subsets by flow cytometry. Each data point represents one mouse, with at least three biological replicates for all panels. Data in (C) were analyzed by unpaired t test, whereas data in (F to H) were analyzed by one-way ANOVA with Tukey's multiple comparisons test. Data with no indicated P values were not significant (P > 0.05). Error bars represent means \pm SD.

Fig. 4. Immune cells may be a source of heparanase during psoriasis-like skin inflammation. (A to E) Mice were left untreated or were treated topically with Aldara cream to the ear pinnae for 6 days. The amounts of heparanase were measured by ELISA in the blood (A) and skin (B). (C) Intracellular heparanase expression in skin leukocytes was measured by flow cytometry. (D) Representative flow cytometry plots of monocyte heparanase staining. (E) The percentages of monocytes positive for heparanase over the indicated time of Aldara cream treatment. (F) Bone marrow cells were cultured in the presence of IL-17, imiquimod (IMQ), or both, for 3 days, and the amounts of heparanase secreted into the medium were measured by ELISA. Each data point represents one mouse, except for (E and F), with at least three biological replicates for all panels. Data in (A and B) were analyzed by unpaired *t* test, whereas data in (E and F) were analyzed by one-way ANOVA with Tukey's multiple comparisons test. Error bars represent means ± SD.

Fig. 5. A HS mimetic reduces HS loss from leukocytes in response to skin inflammation, inhibiting their accumulation in skin, but increasing clinical signs of inflammation. (A to J) Mice were treated topically with 10 mg of Aldara cream to the ear

pinnae daily for 6 days (day 0 to 5), together with i.p. injection of PBS or the HS mimetic, Tet-29, daily for 7 days (days -1 to 5) (A). (B) Total CD45+ cells were stained for HS and analyzed by flow cytometry. (C) The amounts of HS in the blood were measured by ELISA. (D) Clinical signs of inflammation were monitored by measuring ear thickness with a calipers and visually scoring ear redness and ear scaling. (E and F) Skin was sectioned and stained with H&E (E), and epidermal thickness was measured from images and calculated as a percentage of total ear thickness (F). Scale bars, 100 µm. (G to I) Flow cytometry was used to determine the total numbers of CD45+ cells in ear skin were quantified (G), as well as numbers of macrophages, monocytes, DCs, T cells, and neutrophils (H), and Treg cells (I). (J) The amounts of IL-10 in the skin were measured by ELISA and noramlized to the amounts in the skin of control (PBS-treated) mice. (K and L) Mice were treated with a T_{req} cell–depleting antibody (anti-CD25) during the course of Aldara cream treatment. (K) Ear thickness was measured using calipers, and ears were visually scored for redness and scaling. (L) Aldara and anti-CD25 treated skin was also stained by H&E, and epidermal thickness was calculated as a percentage of total ear thickness. Each data point represents one mouse, with at least three biological replicates for all panels. Data in (B, D, F to I, K, and L) were analyzed by two-way ANOVA with Tukey's multiple comparisons test, except for the redness and scaling measurements, which were discontinuous variables and thus were analyzed by Kruskal-Wallis with Dunn's multiple comparisons. Data in (C and J) were analyzed by unpaired t test. Error bars represent means ± SD. AU, arbitrary units. *** denotes P<0.001 and **** denotes P<0.0001.

Fig. 6. Degradation of HS on the surface of monocytes increases their ability to migrate and adhere to endothelial cells. (A and B) Mouse bone marrow cells were cultured with or without heparinase I and III to degrade cell surface HS, which confirmed by flow cytometry analysis (A) and quantified (B). (C and D) Control and heparinase-treated immune cells were co-cultured with an endothelial cell monolayer (C), before being washed off and the adhered cells being quantified (D). (E and F) The migratory ability of monocytes was tested by allowing medium-treated and heparinase-treated cells to migrate toward the chemokine CCL7 for 2 hours (E) and then counting the percentage of total monocytes that had migrated (F). At least three biological replicates are shown for all panels. Data were analyzed by unpaired *t* test. Error bars represent means ± SD.

Fig. 7. HS shedding from the glycocalyx of leukocytes enables their infiltration into the skin during psoriasis-like skin inflammation. We propose that the leukocyte glycocalyx acts as a barrier to migration and is shed during inflammation, which enables the cells to then migrate to inflammatory sites. Adapted from Sutherland *et al.* (7).

Figure 1

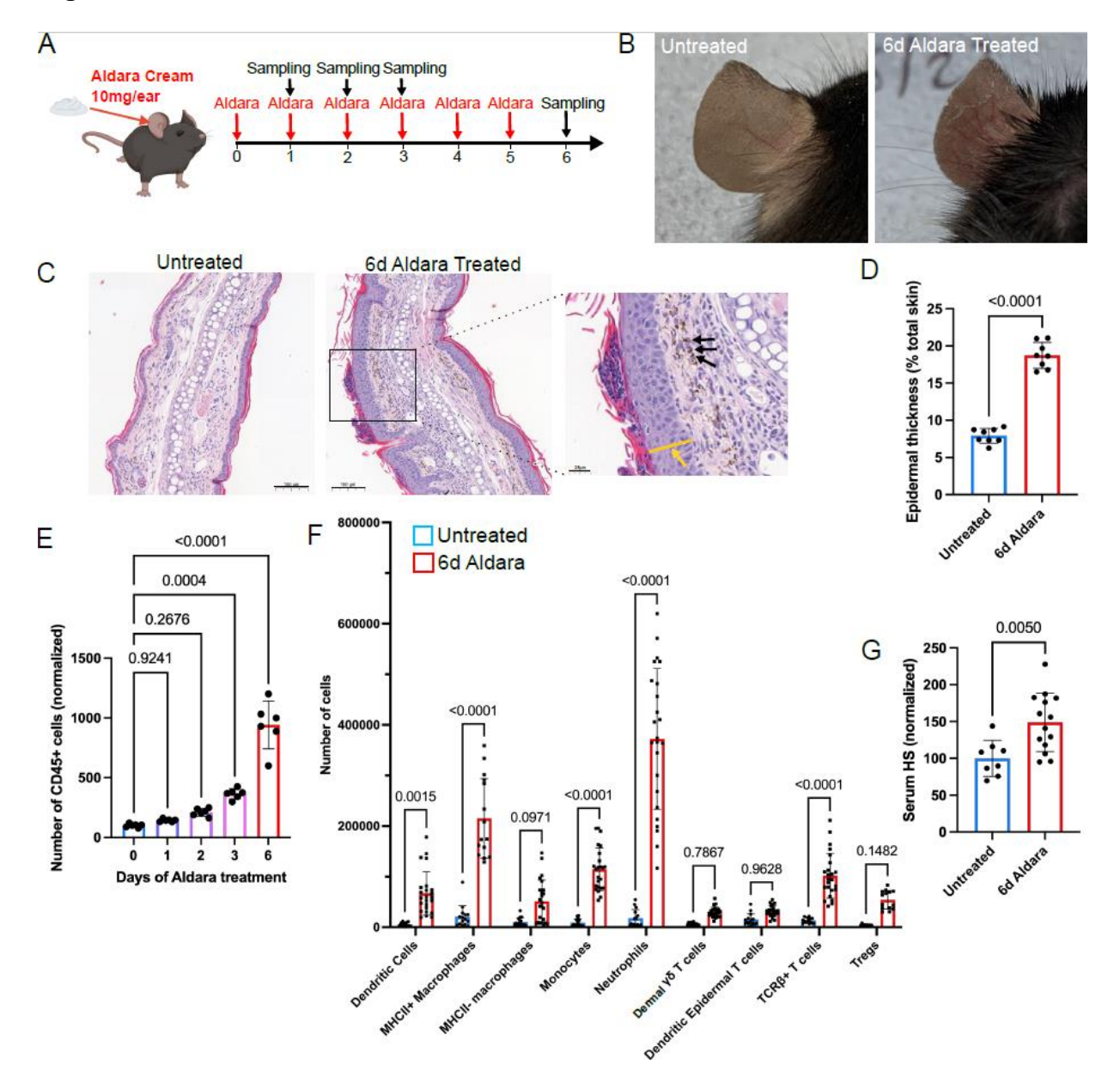


Figure 2

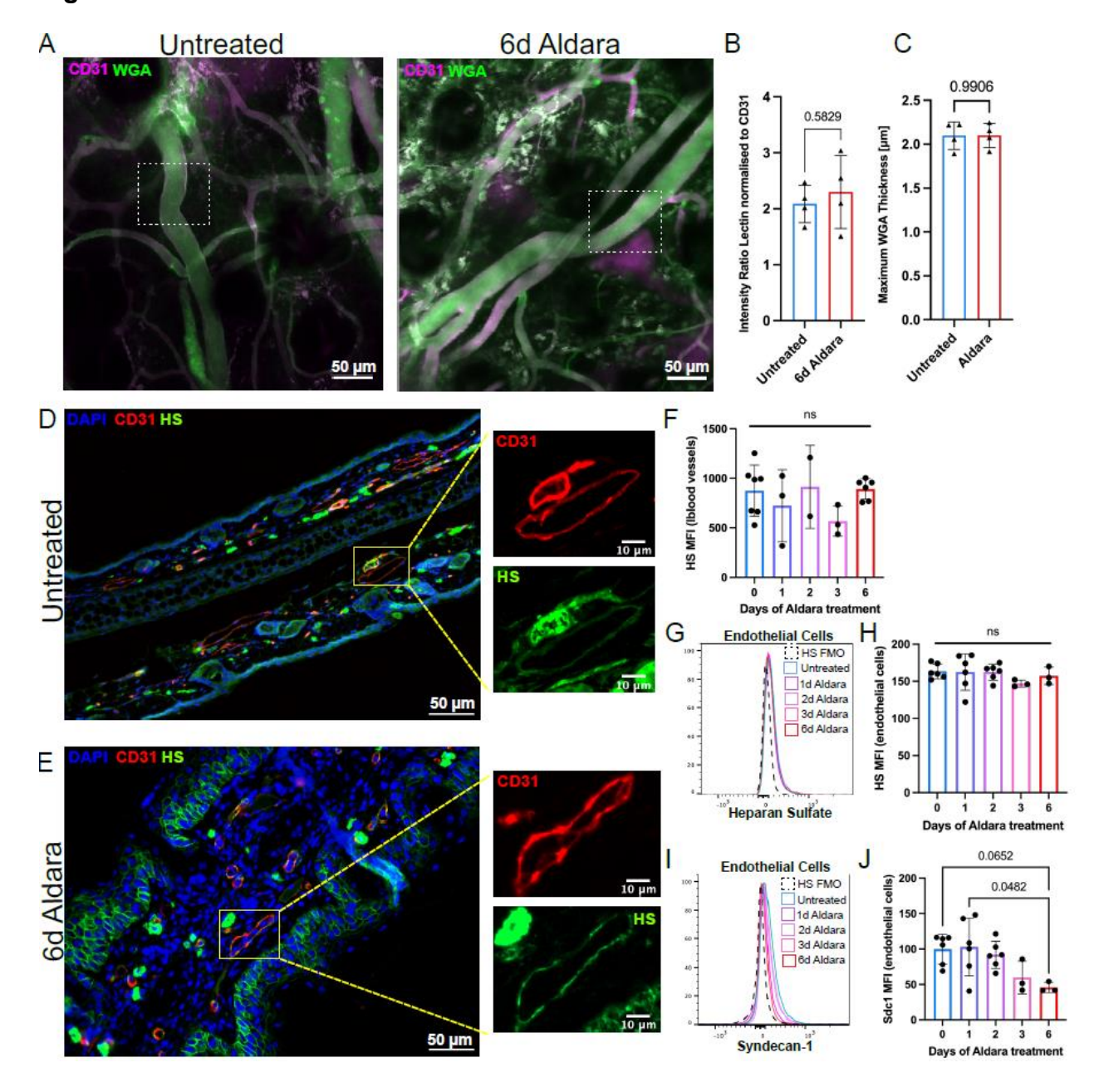


Figure 3

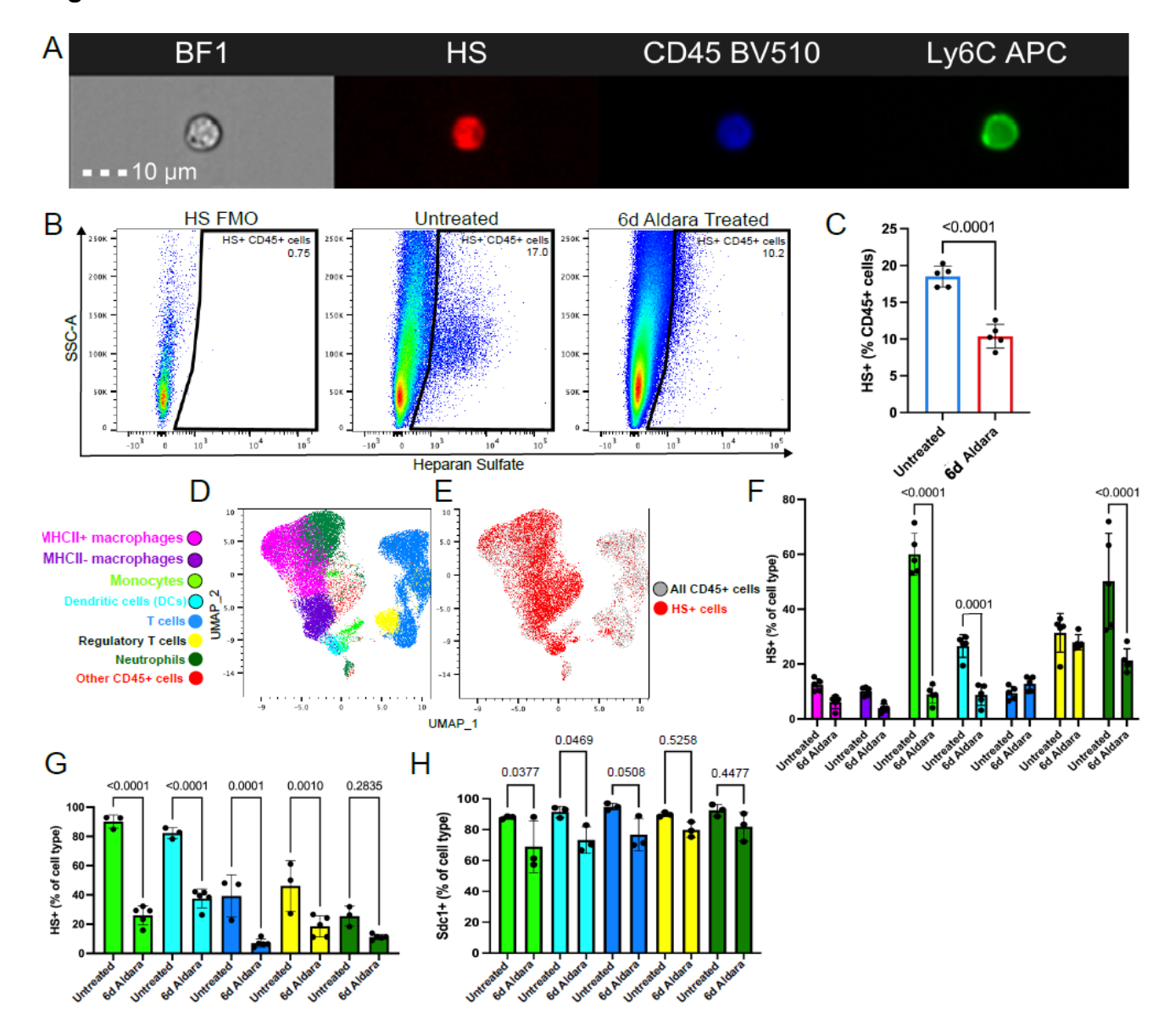


Figure 4

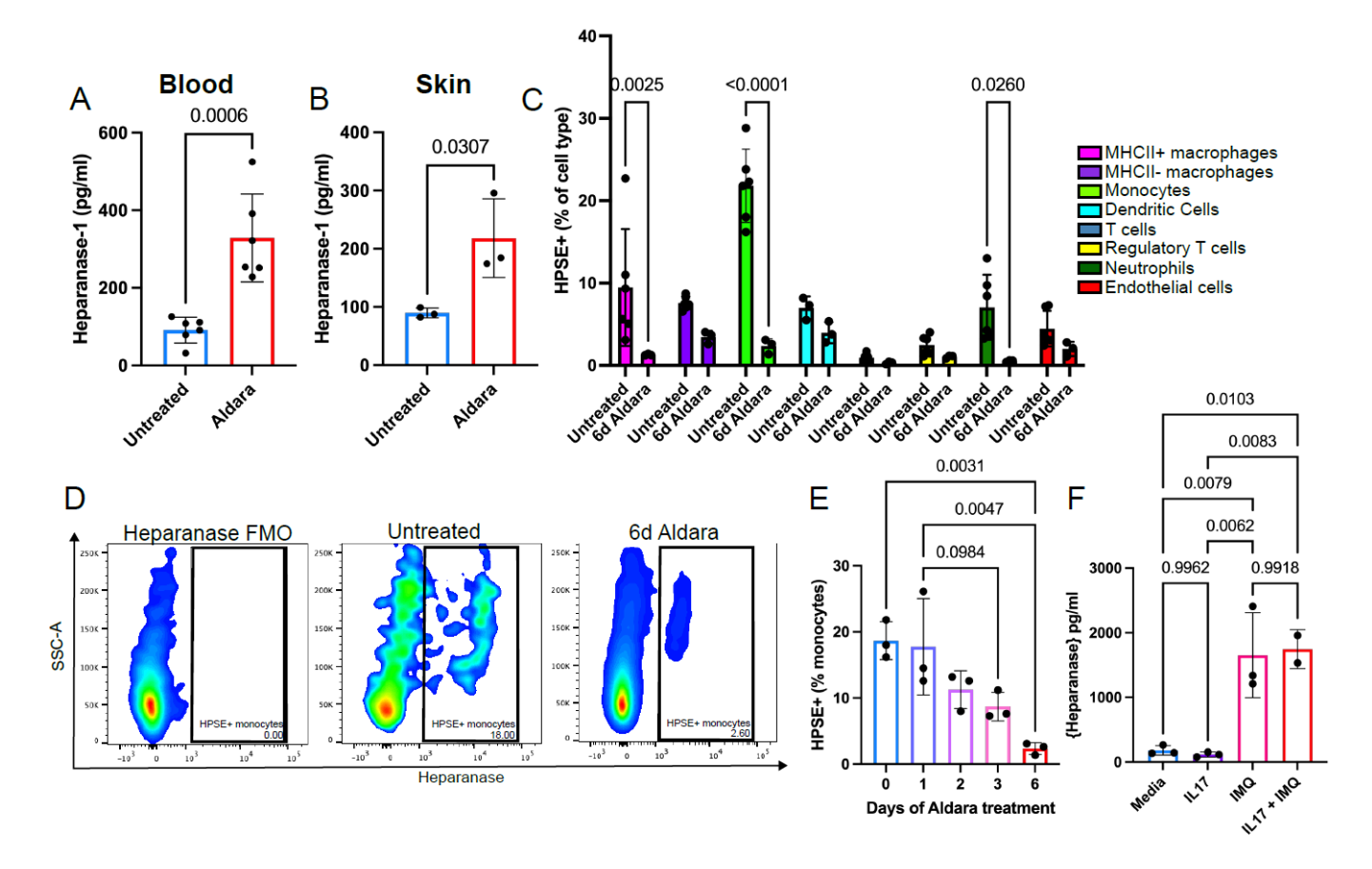


Figure 5

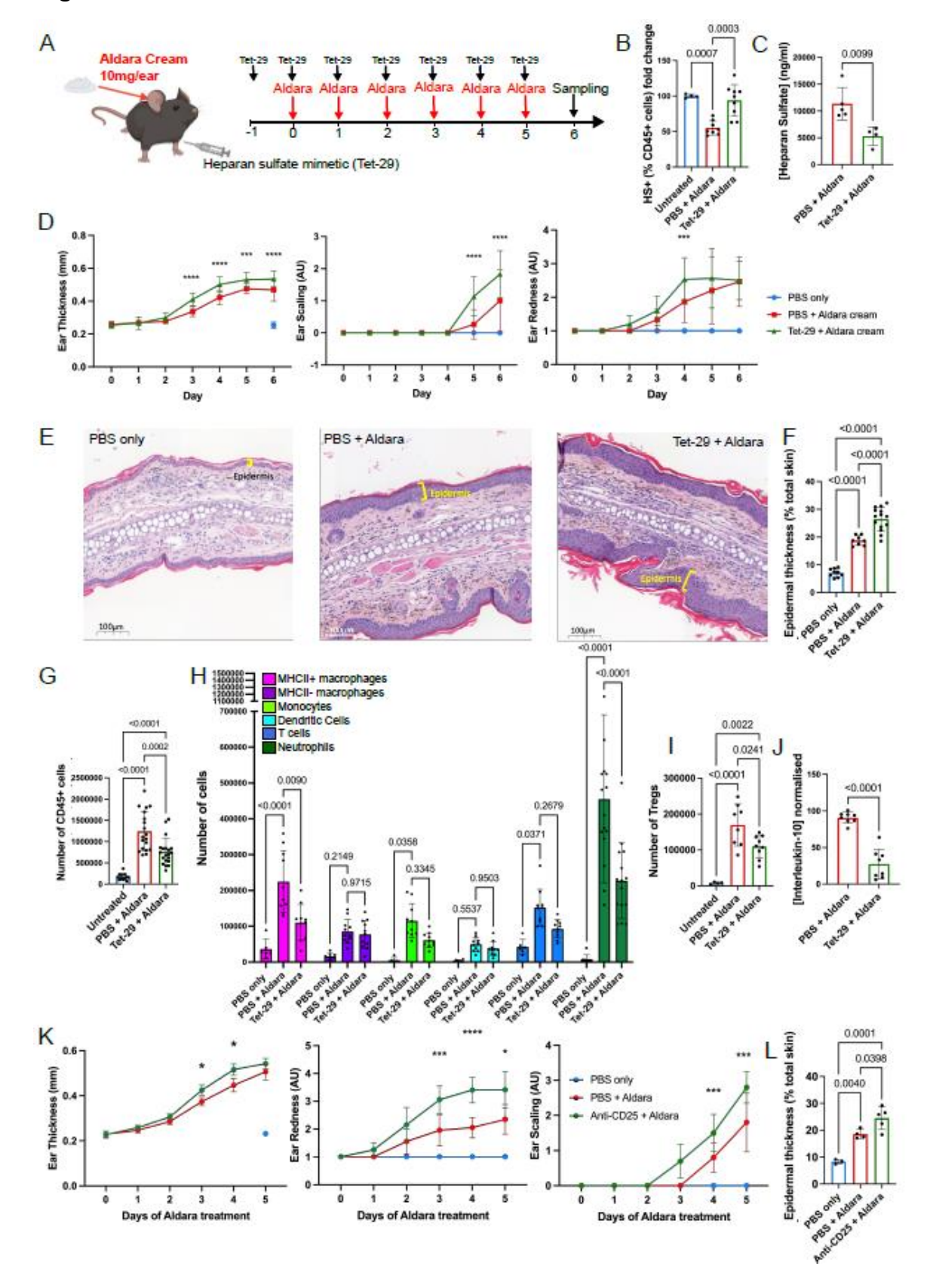


Figure 6

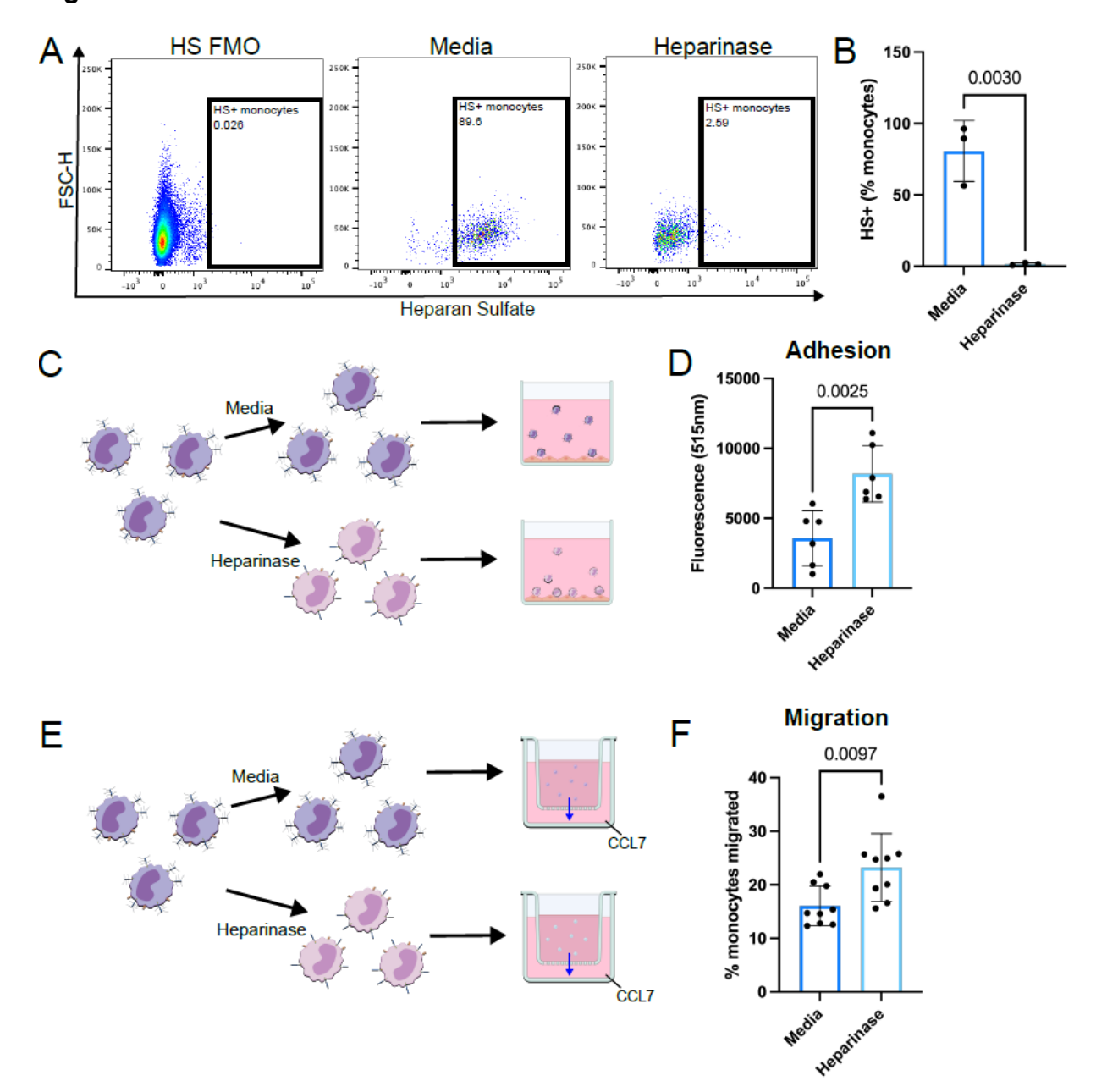
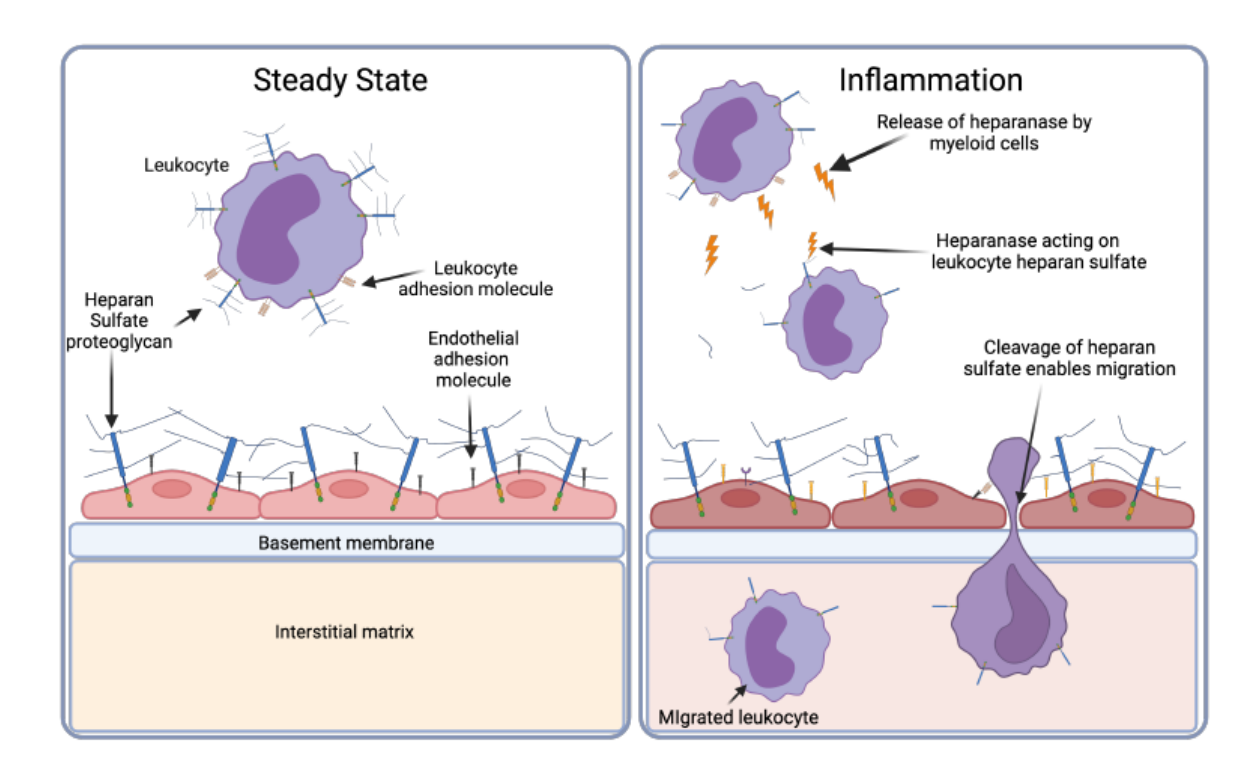


Figure 7



Supplementary material < 0.0001 C Α В < 0.0001 < 0.0001 <0.0001 <0.0001 0.0046 < 0.0001 < 0.0001 >0.9999 < 0.0001 Ear Thickness (mm) Ear Scaling (AU) Redness (AU) 3 0.8144 >0.9999 0.2248 0.9953 >0.9999 >0.9999 Ear 0.0 2 3 2 3 4 5 1 2 3 4 5 **Days of Aldara treatment** Days of Aldara treatment Days of Aldara treatment Untreated 3d Aldara 50µm 0.0001 6d Aldara 0.0037 Ε (normlaised) 0.0024 0.0530 0.0077 0.0240 0.2254 CD31+ % skin cells Number of endothelial

50µm

Fig. S1. Characterizing changes in clinical signs of inflammation and the vasculature during psoriasis-like skin inflammation. (A to F) Mice were treated topically with 10 mg of Aldara cream to each ear pinnae daily for 0 to 6 days. (A to C) Clinical signs of inflammation were quantified by measuring ear thickness (A) and scoring redness (B) and scaling (C) against a scale. (D and E) Skin was sectioned and stained for DAPI (blue) and CD31 (red) as a marker of endothelial cells (D), and the vascularization of the tissue was quantified by calculating the percentage of the skin that was positive for CD31 staining (E). Scale bars, 50 µm. (F) The number of endothelial cells was quantified by staining the skin for CD31 by flow cytometry and normalizing to the mean of the untreated controls. Each data point represents one mouse with at least three biological replicates for all panels. Data in (A, E, and F) were analyzed by one-way ANOVA with Tukey's multiple comparison test. Data in (B and C) are discontinuous variables and so were analyzed by non-parametric Kruskal-Wallis test with Dunn's multiple comparison test. Data in (A to C) show significant differences compared to untreated mice (day 0) only. Data in (E and F) with no P values were not significant (P > 0.05). Error bars represent means \pm SD. AU, arbitrary units.

3d Aldara

2

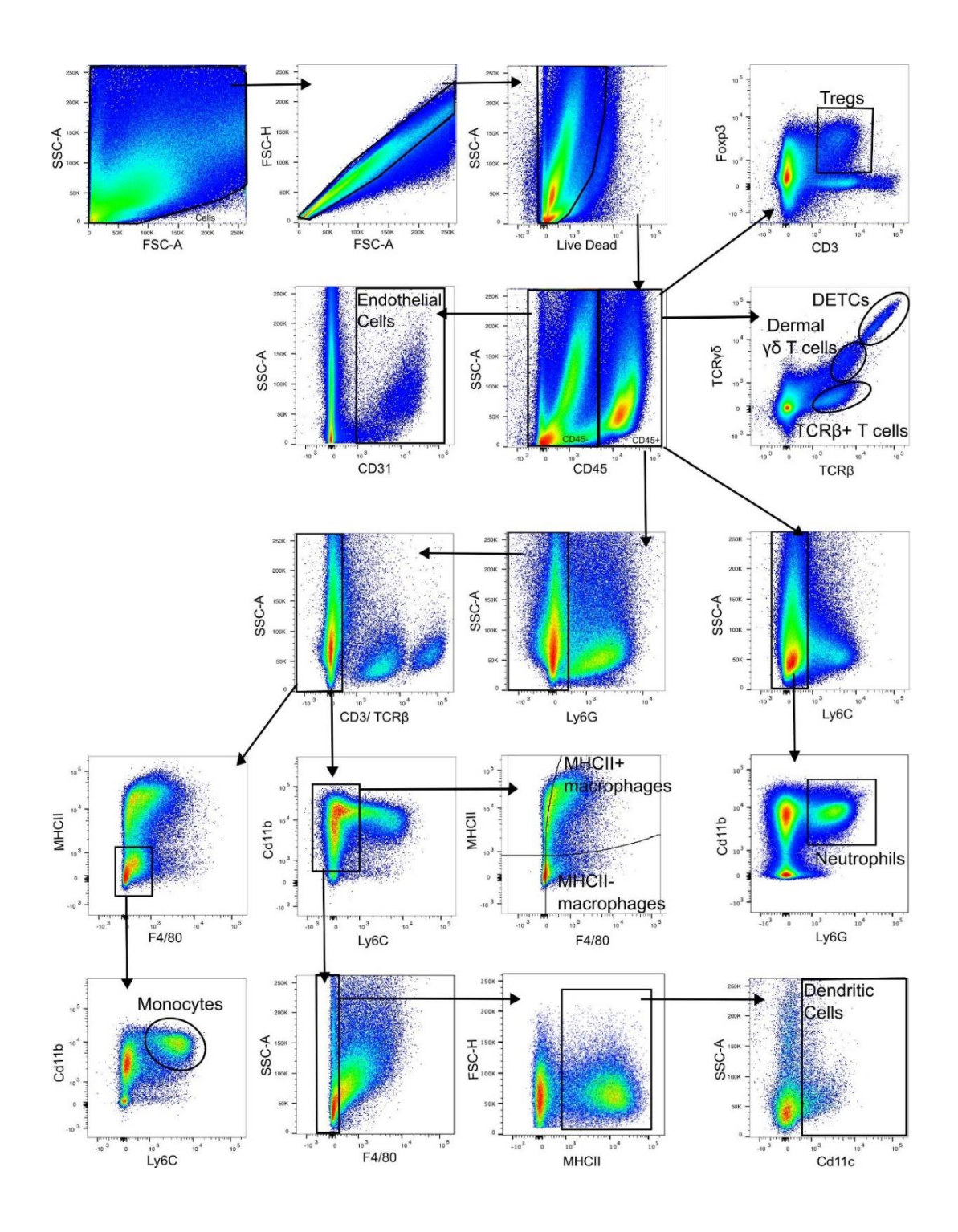


Fig. S2. Flow cytometry gating strategy for skin leukocytes and endothelial cells. Cells were gated based on forward scatter (FSC) and side scatter (SSC) characteristics, and then single cells were gated based on the linearity of the FSC-A versus FSC-H parameters. Live cells were gated as LiveDead⁻. Endothelial cells were gated as CD45⁻ CD31⁺. Immune cells were gated as CD45⁺, followed by subsequent gating into the indicated subsets.

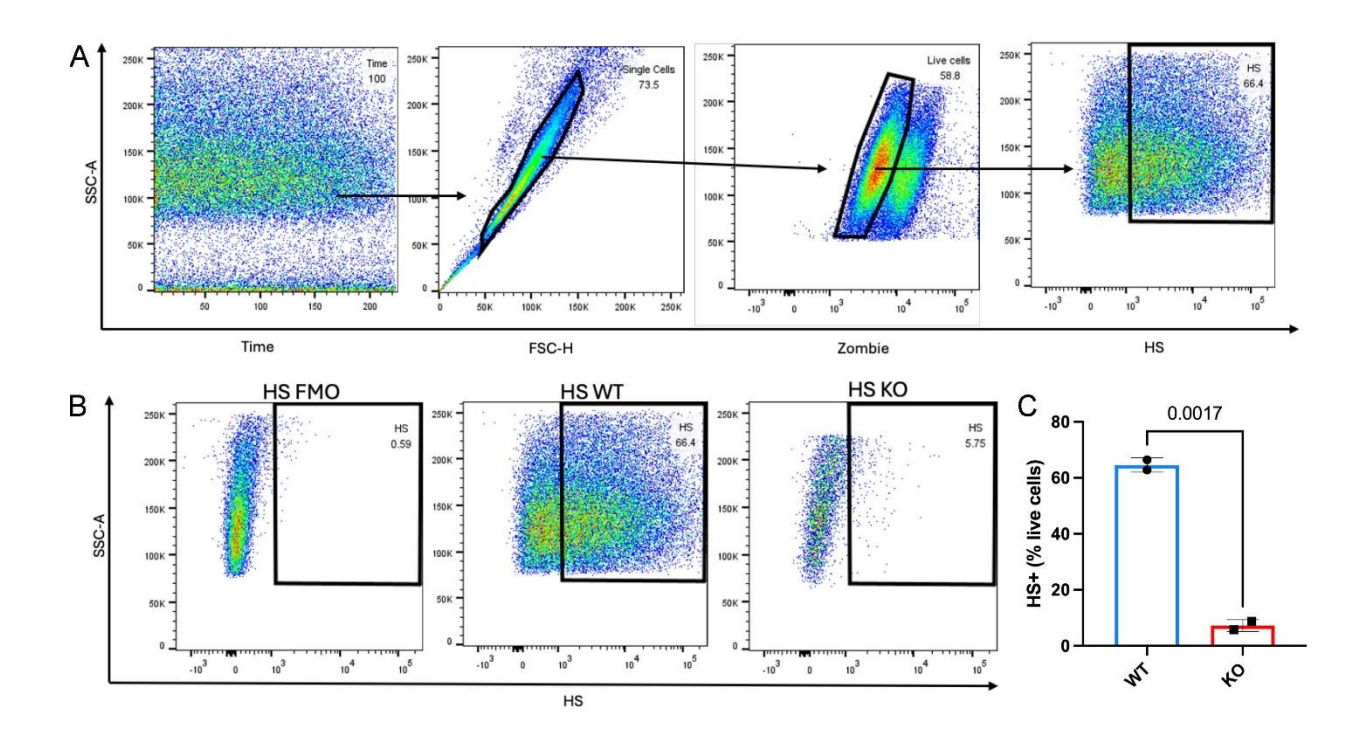


Fig. S3. The 10e4 anti-HS antibody binds to HS. (A to C) Wild-type (WT) and heparan sulfate knock out (KO) CHO cells were stained with an anti-HS antibody for flow cytometric analysis (A and B). The percentages of cells expressing HS were then quantified (C). Data were analyzed by unpaired t test, with at least two biological replicates for all panels. Error bars represent means \pm SD.

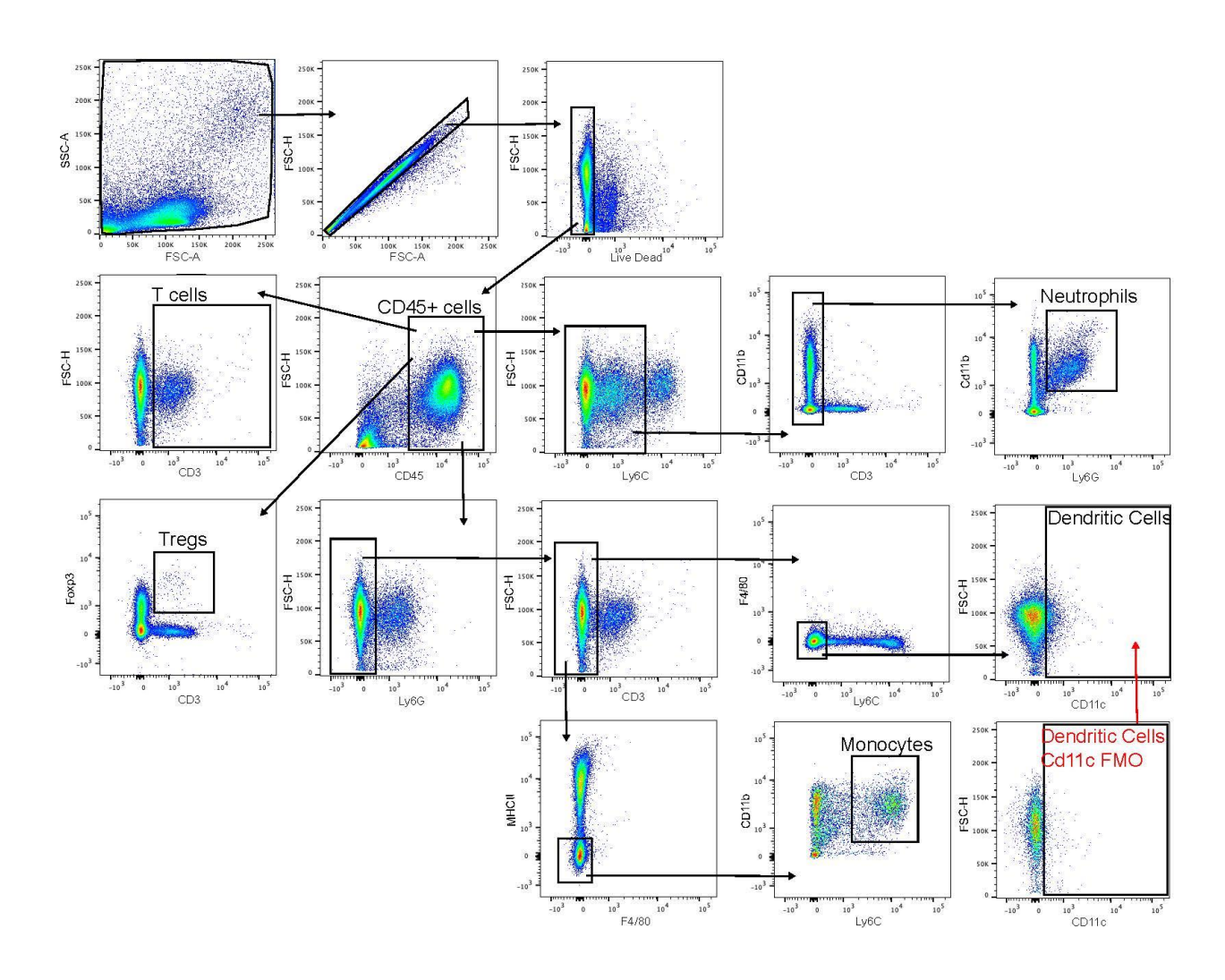


Fig. S4. Flow cytometry gating strategy for blood leukocytes. Cells were gated based on FSC and SSC characteristics, and then single cells were gated based on the linearity of the FSC-A versus FSC-H parameters. Live cells were gated as LiveDead⁻. Immune cells were gated as CD45⁺, follow by subsequent gating into the indicated subsets.

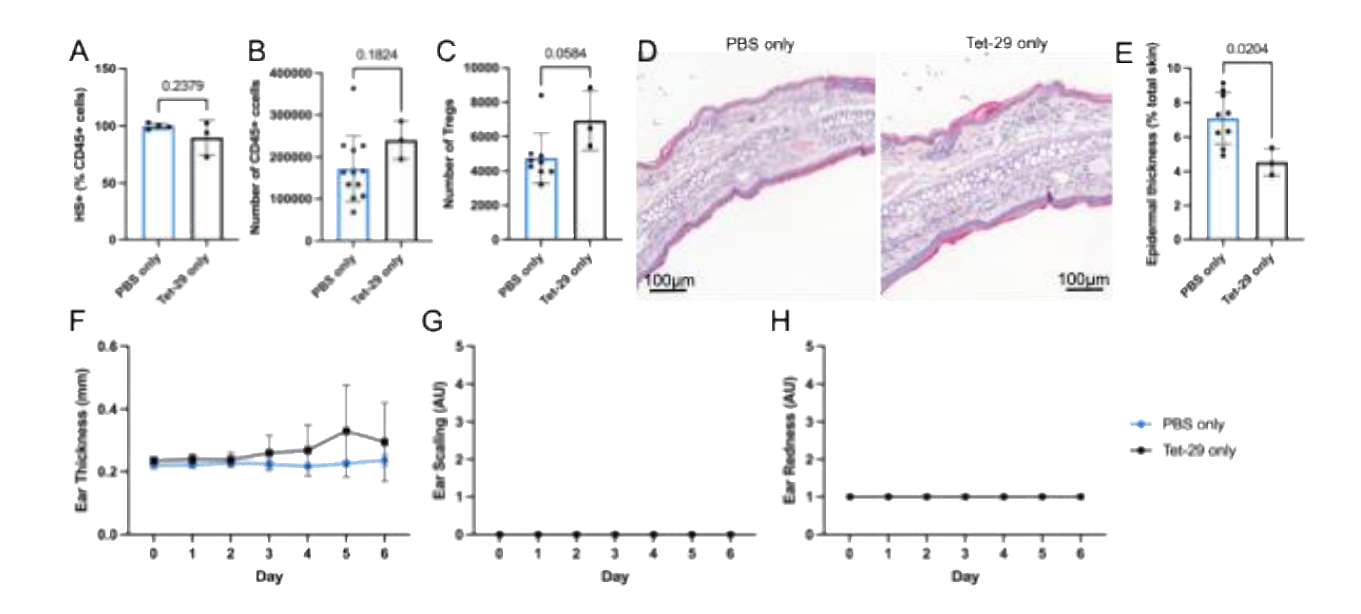


Fig. S5. The effects of Tet-29 on resting skin. (A to H) Mice were injected i.p. with either PBS or the HS mimetic, Tet-29, daily for 7 days. (A to C). The percentages of leukocytes expressing HS (A), the numbers of CD45⁺ cells (B), and the numbers of T_{reg} cells (C) in the skin were determined by flow cytometry. (D and E) Skin sections were stained with H&E (D), and epidermal thickness was measured as a proportion of total ear thickness (E). Scale bars, 100 μm. (F to H) Clinical signs of inflammation were monitored by measuring ear thickness with calipers (F), and the visually scoring ear scaling (G) and ear redness (H). Each data point shows one mouse with at least three biological replicates for all panels. Data in (A to E) were analyzed by unpaired t test, data in (F) were analyzed by two-way ANOVA with Tukey's multiple comparisons, and data in (G and H) were analyzed by Kruskal-Wallis with Dunn's multiple comparisons. Error bars represent means \pm SD. AU, arbitrary units.

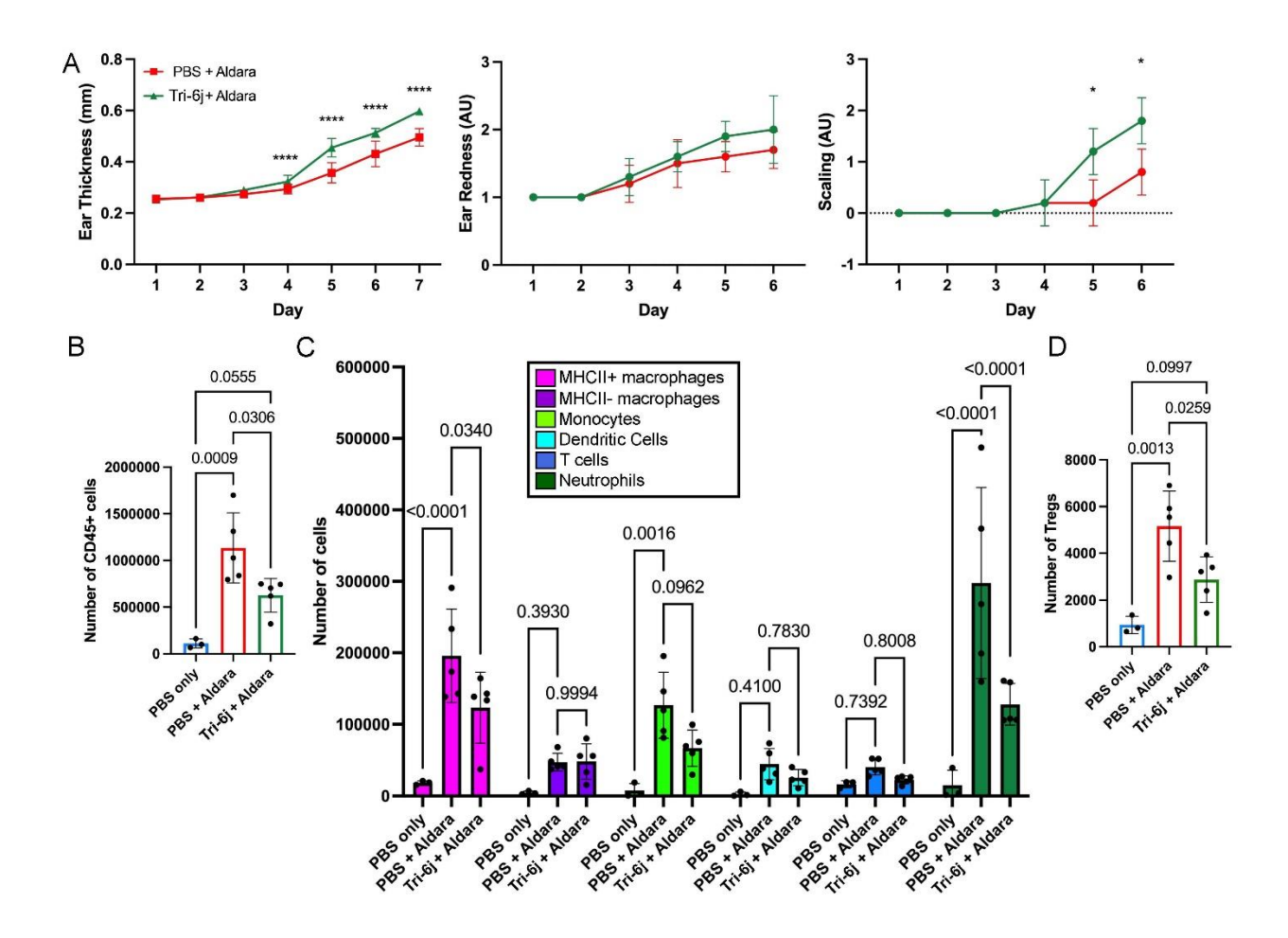


Fig. S6. A second HS mimetic inhibits leukocyte recruitment in skin but increases clinical signs of inflammation. (A to D) Groups of mice were treated with topical application of 10 mg of Aldara cream to the ear pinnae daily for 6 days (days 0 to 5) together with i.p. injection of a HS mimetic, denoted as "Tri-6j," daily for 7 days (days 1 to 5) or PBS as a control. (A) Clinical signs of inflammation were monitored by measuring ear thickness with calipers and visually scoring ear redness and ear scaling. (B to D) Quantification of the total numbers of CD45 $^+$ cells (B), macrophages, monocytes, DCs, T cells, and neutrophils (C), and T_{reg} cells (D). Each data point shows one mouse with at least three biological replicates for all panels. Data in (A and C) were analyzed by two-way ANOVA with Tukey's multiple comparisons test, except for the redness and scaling measurements which are discontinuous variables and so were analyzed by Kruskal-Wallis with Dunn's multiple comparisons. Data in (B and D) were analyzed by two-way ANOVA with Tukey's multiple comparisons test. Error bars represent means \pm SD. AU, arbitrary units.

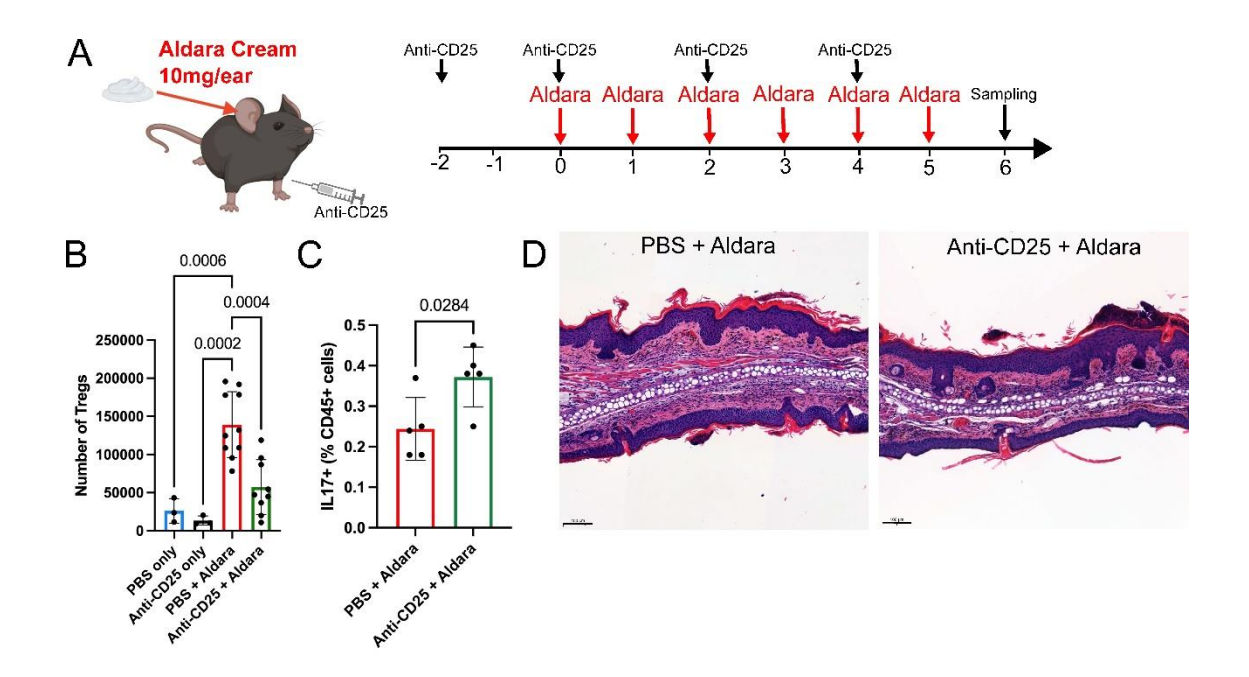


Fig. S7. Anti-CD25 treatment depletes T_{reg} cells and exacerbates some signs of inflammation during psoriasis-like skin inflammation. (A to D) Mice were treated daily with topical application of Aldara cream to the ear pinnae (days 0 to 6) together with i.p. injection of an anti-CD25 antibody on days -2, 0, 2, and 4 (A), leading to the depletion of T_{reg} cells in the skin, as measured by flow cytometry (B). (C) Eardraining (auricular) lymph nodes were analyzed by flow cytometry, and the percentage of CD45⁺ cells producing IL-17 were quantified. (D) Skin was sectioned and subjected to H&E staining. Scale bars, 100 μ m. Each data point represents one mouse with at least three biological replicates for all panels. Data were analyzed by one-way ANOVA and Tukey's multiple comparison test, except for the data in (C), which were analyzed by unpaired t test. Error bars represent means \pm SD.

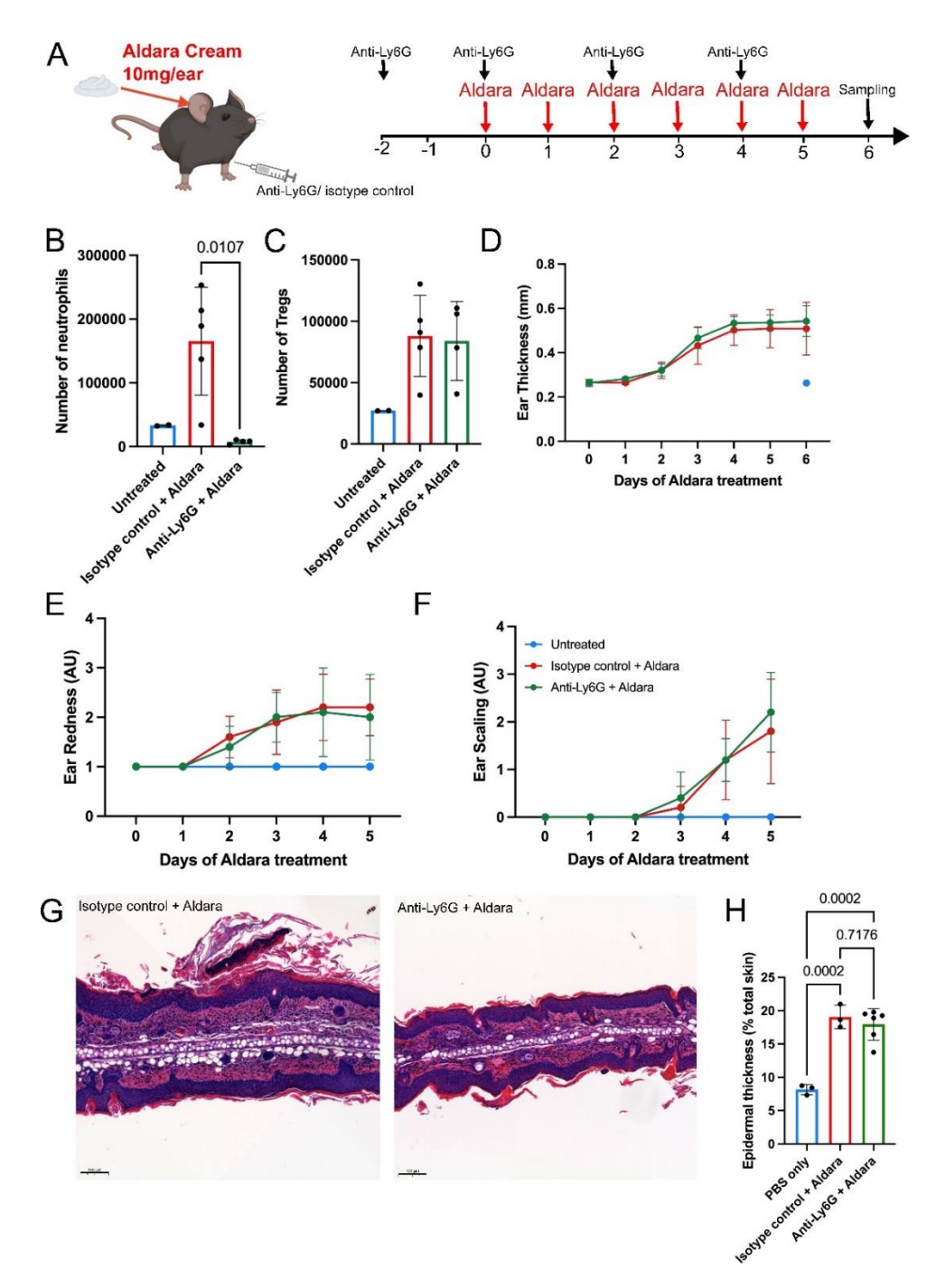


Fig. S8. Depletion of neutrophils does not recapitulate the enhanced inflammation caused by heparanase inhibition during psoriasis-like skin inflammation. (**A** to **H**) Mice were treated daily with topical application of Aldara cream to the ear pinnae (days 0 to 6) together with i.p. injection of an anti-Ly6G antibody on days -2, 0, 2, and 4 (A), leading to the depletion of neutrophils in the skin as measured by flow cytometry (B). (C) The numbers of T_{reg} cells in two ears were measured by flow cytometry. (D to F) Clinical readouts of inflammation were scored, including ear thickness (D), redness (E), and scaling (F). (G and H) Skin was sectioned and stained with H&E (G), and epidermal thickness was measured and calculated as a percentage of the total ear thickness (H). Scale bars, 100 μm. Each data point represents one mouse, with at least three biological replicates for all panels. Data were analyzed by one-way ANOVA and

Tukey's multiple comparison test, except for data in (E and F), which are discontinuous variables and so were analyzed by non-parametric Kruskal-Wallis test with Dunn's multiple comparisons. Data with no P values were not significant (P > 0.05). Error bars represent means \pm SD.

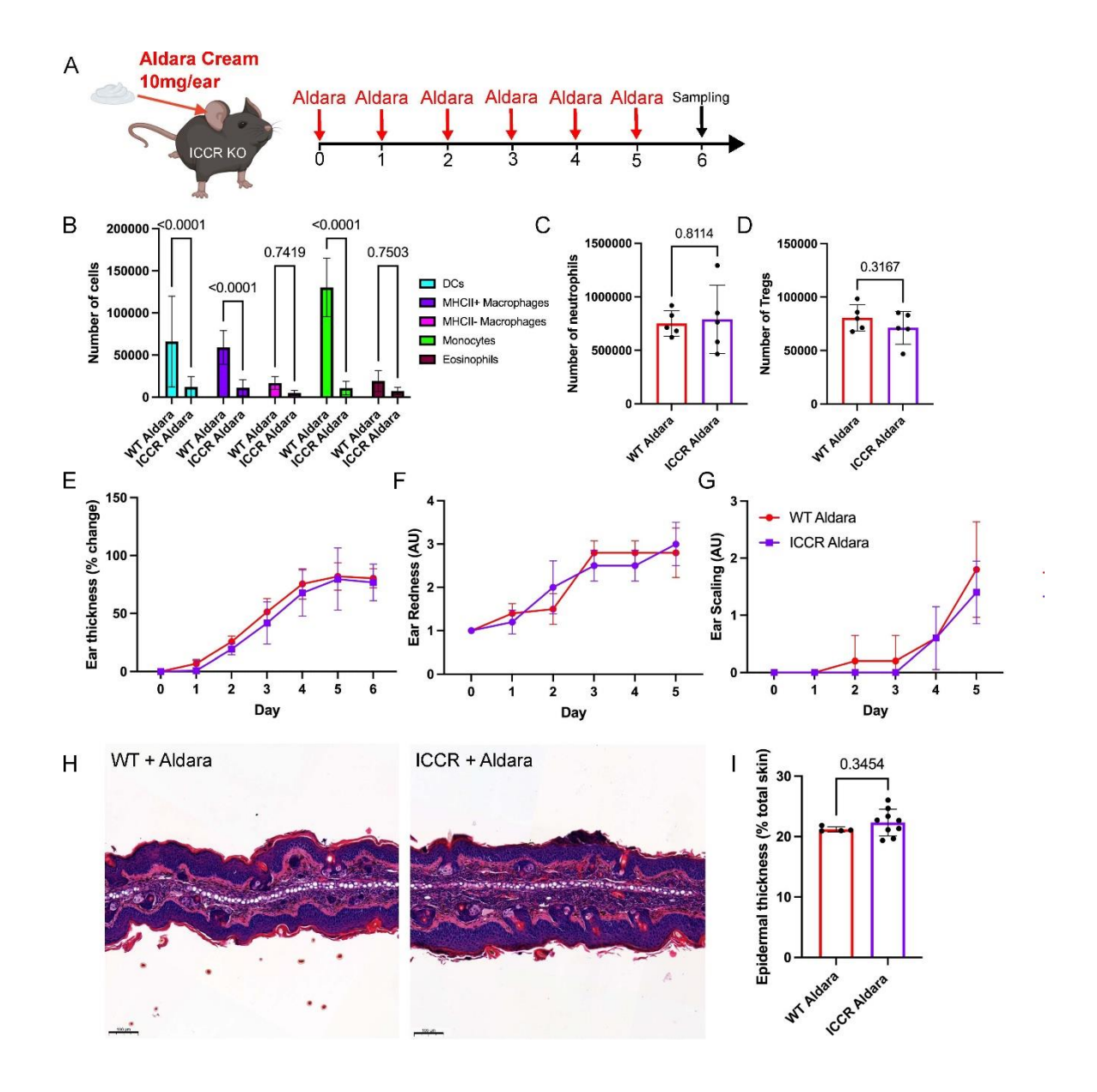


Fig. S9. Depletion of myeloid cells does not recapitulate the exacerbated inflammation seen with heparanase inhibition during psoriasis-like skin inflammation. (A to I) ICCR KO mice and WT littermate controls were treated daily with topical application of Aldara cream to the ear pinnae for 6 days (A). The numbers of DCs, macrophages, monocytes, and eosinophils (B), as well as neutrophils (C), and T_{reg} cells (D) in the skin were quantified by flow cytometry. (E to G) Clinical readouts of inflammation were measured, including ear thickness (E), redness (F), and scaling (G). (H and I) Skin was sectioned and stained with H&E (H), and epidermal thickness was measured and calculated as a percentage of the total ear thickness (I). Scale bars, 100 µm. Each data point represents one mouse, with at least three biological replicates for all panels. Data in (B and E) were analyzed by one-way ANOVA and Tukey's multiple comparison test. Data in (F and G) are discontinuous variables and so were analyzed by non-parametric Kruskal-Wallis test with Dunn's multiple comparisons. Data in (C, D, and I) were analyzed by unpaired t test. Data with no P values were not significant (P > 0.05). Error bars represent means \pm SD.

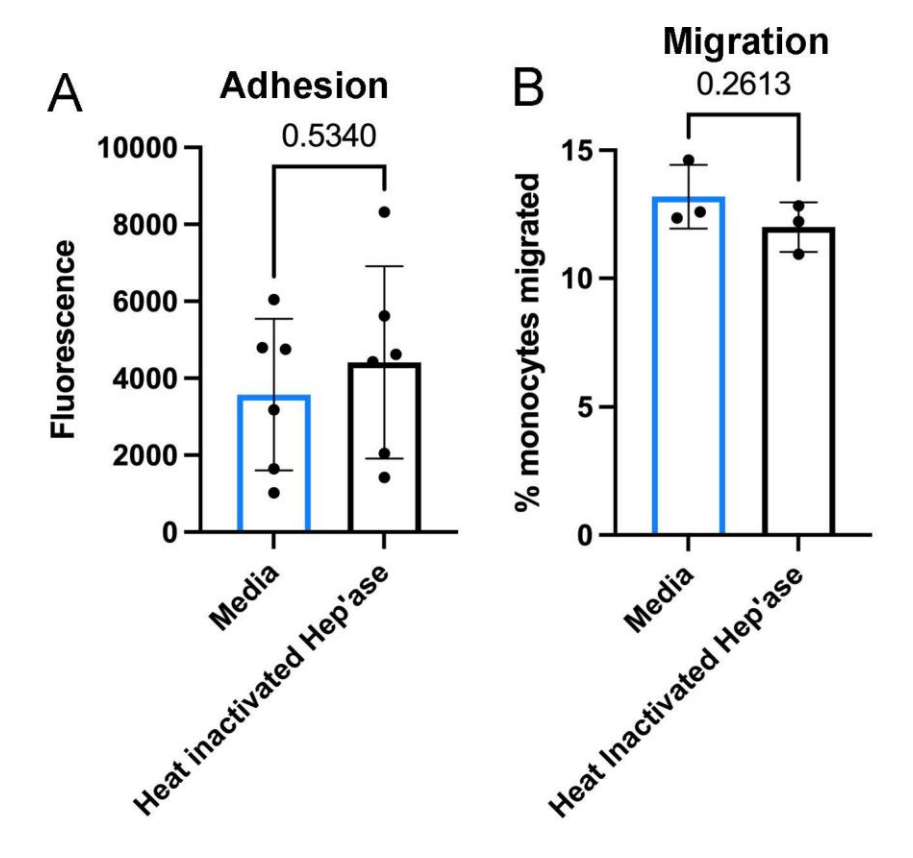


Fig. S10. Heat-inactivated controls for in vitro adhesion and migration experiments. (A and B) Mouse bone marrow cells were cultured with or without heat-inactivated heparinase I and III. (A) The cells were then co-cultured with an endothelial cell monolayer, before being washed off, and the adhered cells were then quantified. (B) The migratory ability of the cells was tested by allowing cells treated with medium and or heat-inactivated heparinase to migrate toward CCL7 and counting the percentage of total monocytes that migrated. Data are from at least three biological replicates and were analyzed by unpaired t tests. Error bars represent means \pm SD.

Table S1. Antibodies used for flow cytometry analysis.

Antigen	Conjugate	Dilution	Clone	Supplier
CD11b	FITC	1:300	M1/70	eBioscience
CD11c	BV605	1:800	N418	BioLegend
CD3	APC-Cy7	1:100	17A2	eBioscience
CD31	BV711	1:200	390	BD Biosciences
CD45	BV510	1:300	30-F11	BioLegend
F4/80	BV786	1:500	BM8	BioLegend
Fc block (CD16/CD32)	Unconjugated	1:1000	2.4G2	BD Bioscences
Foxp3*	BV421	1:100	FJK-16s	eBioscience
Heparan Sulfate	Biotin	1:200	F58-10E4	Amsbio
Heparanase*	None (Rabbit IgG)	1:200	N/A	Proteintech
IL-17*	PE-Cy7	1:100	eBio1787	eBioscience
Ly6C	PerCPCy5.5	1:500	HK1.4	BioLegend
Ly6C	APC	1:100	HK1.4	BioLegend
Ly6G	AF700	1:200	1A8	BioLegend
MHCII	BV650	1:500	MS/114.15.2	BioLegend
Siglec F	PEef610	1:400	E50-2440	BD Biosciences
Streptavidin	PEef610	1:200	N/A	BioLegend
TCRβ	APC-Cy7	1:200	H57-597	eBioscience
ΤCRγδ	APC	1:300	GL3	eBioscience
Rabbit IgG	PE	1:200	Polyclonal	Rockland

^{*}Antibody against intracellular target.

#Stained overnight

Table S2. Antibodies used for immunofluorescence.

Reagent	Conjugate	Dilution	Target	Species	Clone	Supplier
Mouse anti-HS	Unconjugated	1:250	НН	Mouse	F58- 10E4	Amsbio
M.O.M. biotinylated anti-mouse IgG reagent	Biotin	1:200	Primary anti-HS antibody	N/A	N/A	Vector
Streptavidin	NL-557	1:800	Biotin on secondary antibody	N/A	N/A	R&D systems
Rabbit anti- CD31	Unconjugated	1:50	Endothelial cells	Rabbit	DBV9E	Cell signaling Technology
Donkey anti- rabbit IgG	NL-637	1:100	Primary CD31 antibody	Donkey	N/A	R&D systems